DISSERTATION

On

Bond Graph aided Performance Analysis of Antilock Braking System for a Vehicle with Camber and Fork Angle

Submitted in partial fulfillment of the requirement

for the award of degree of

Master of Engineering

in

Thermal Engineering

Submitted By :

ADITYABIR SINGH

Roll No. 801183002

Under The Guidance of

Dr. Tarun Kumar Bera

Assistant Professor

Department of Mechanical Engineering

Thapar University, Patiala

DEPARTMENT OF MECHANICAL ENGINEERING

THAPAR UNIVERSITY

PATIALA-147004, INDIA

JULY-2013

"IF THE ONLY PRAYER YOU SAY IN YOUR ENTIRE LIFE IS THANK YOU, THAT WILL BE ENOUGH"

This Thesis is dedicated to my Supervisor

Dr. Tarun Kumar Bera

for his infinite kindness and patience

DECLERATION

I hereby declare that work done in this Thesis Report entitled, **"Bond Graph aided Performance Analysis of Antilock Braking System for a Vehicle with Camber and Fork Angle"** submitted towards partial fulfilment of requirement for award of **Master of Engineering** degree in **Thermal Engineering** in **Mechanical Engineering Department** of **Thapar University, Patiala,** is an authentic record of work carried out by me under the supervision and guidance of **Dr. Tarun Kumar Bera, Assistant Professor** of **Mechanical Engineering Department, Thapar University, Patiala.**

This matter embodied in this report has not been submitted in part or full to any other university or institute for the award of any degree.

Adityabir Singh

Adityabir Singh

This is to certify that above declaration made by the student concerned is correct to the best of my knowledge & belief.

Dr. Tarun Kumar Bera
Assistant Professor
Mechanical Engineering Department
Thapar University, Patiala

Countersigned by:

Dr. Ajay Batish
Professor & Head of the Department
Mechanical Engineering Department
Thapar University, Patiala

Dr. S.K. Mohapatra
Sr. Prof & Dean of Academic Affairs
Mechanical Engineering Department
Thapar University, Patiala

ACKNOWLEDGEMENT

I take the opportunity to express my heartfelt adulation and gratitude to my supervisor Dr. Tarun Kumar Bera for his unreserved guidance, constructive suggestions, thought provoking discussions and unabashed inspiration in the nurturing work. It has been a benediction for me to spend many opportune moments under the guidance of the perfectionist at the acme of professionalism. The present work is testimony to his activity, inspiration and ardent personal interest, taken by him during the course of his work in its present form. I am grateful to Dr. Ajay Batish, Professor and Head, Mechanical Engineering Department for providing the facilities for the completion of the work and always being a shelter in the odd days.

No words acknowledge the support that I received from my friends and family. I would like to thank all my family members and friends for there affectionate blessings and help. I would like to thank all the members and employees of Mechanical Engineering Department, Thapar University, Patiala. In express my indebtedness to the 'ALMIGHTY' for all his blessing and kindness.

Adityabir Singh

Adityabir Singh

801183002

M.E. Thermal

ABSTRACT

The 21st century vehicle on the road is expected to have such features which not only increase the comfort and ride quality but also increase the safety of the driver. For the different road surfaces and increase in traffic congestions, the conventional safety systems are unable to provide the desired action. So, there is a need to develop more and more accurate control algorithms which will be effective in every situation.

Due to the ever increase traffic on Indian roads, the most frequently job performed by the driver is to apply the brakes. The braking of the vehicle is not only depends on the driver response, but also takes into number of factors like road-tyre friction coefficient, slip ratio, longitudinal tyre force, longitudinal velocity and lateral tyre force. Control of all these parameters is not done by the driver alone. So, some controllers must be developed for assisting the driver to avert such situations.

Sudden application of the brake torque increases the slip ratio which will cause skidding of the wheels. Antilock braking system is a type of braking system which applies and releases the brakes in quick succession to prevent the wheels from locking. Earlier, number of controllers was developed to prevent such lockage. Here, a control algorithm is developed for the brake torque in such a fashion that the slip ratio will be maintained in the desired range.

Normally, the braking of vehicle is done when vehicle in straight path is considered. When vehicle moves in the curved path, the effect of camber and fork angle should be considered. The variable camber angle assists the braking in curved path by increasing the contact path of the tyre with the road. But the turning radius of the vehicle changes due to varying camber angle and fork angle. Fork angle increases the stability of the vehicle at higher speeds.

While turning, the inner wheel always should have positive camber angle and outer wheel should have negative camber angle. Variable camber mechanism is developed to provide the camber angle to the front wheels while moving in a curved path. Variable camber mechanism ensures no camber angle while moving straight ahead to avoid bump steering.

For the analysis, bond graph modelling of various components is done. Quarter car model, Bicycle model and four wheel model of the vehicles are developed. Effect of camber and fork angle on the turning radius, stopping distance and longitudinal speed of the vehicle is analysed. Relation between camber angle and fork angle is also verified. It is also found that camber angle provides additional steering to the vehicle. Analysis of variable camber mechanism is done by using quarter car model.

Control algorithm of Antilock braking system is tested using bicycle model and four wheel vehicle model. The control algorithm successfully keeps

the slip ratio in the acceptable range and thus prevents vehicle skidding and better steering control.

Keywords: Antilock braking system, Camber angle, Fork angle, Variable camber angle mechanism, Bond graph, Quarter car model, Bicycle model, Four wheel model.

LIST OF ABBREVIATIONS

ABS	Antilock Braking System
C	Capacitive Element
CTF	Coordinate Transformation
CVT	Continuously Variable Transmission
EBD	Electronic Brake Distribution
EJS	Euler Junction Structure
GY	Gyrator
I	Inductive Element
PID	Proportional Integral Differential
R	Resistive Element
RCP	Rapid Control Prototyping environment
SCS	Slip Control Strategy
SE	Source of Effort
SF	Source of Flow
SMC	Sliding Motion Controller
TF	Transformer
VC	Virtual Car
VCSS	Variable Camber Suspension System
WDAA	Wheel Deceleration ABS Activation

NOMENCLATURE

a	Distance of front axle from the vehicle cg
b	Distance of front axle from the vehicle cg
B	Stiffness factor
β	Slip angle
C	Shape factor
c	Half of track width
C_{d}	Aerodynamic drag coefficient
D	Peak value
δ	Steering angle
E	Curvature factor
F_{x}	Longitudinal tyre force
F_{y}	Lateral tyre force
F_{d}	Aerodynamic drag force
λ	Fork angle
M_{z}	Self-aligning moment
m_{vb}	Vehicle inertial mass
ϕ	Camber angle
R_{x}	Rolling resistance
r_{t}	Tyre radius
σ_{x}	Slip ratio
$\dot{\theta}_{\mathrm{ty}}$	Tyre angular velocity

SUBSCRIPTS

bd	Brake drum
B	Brake torque
c	Vehicle body
cs	Cable stiffness
c_x, c_y, c_z	x, y, z direction of the vehicle
fn	Front normal
fn	Front tangential
lm	Mechanical losses
rss	Return spring stiffness
s_x, s_y, s_z	x, y, z direction of the suspension
w_x, w_y, w_z	x, y, z direction of the wheel

LIST OF FIGURES

LIST OF TABLES

TABLE OF CONTENTS

CHAPTER 1
INTRODUCTION

1.1 BACKGROUND AND MOTIVATION

Being the second most populous country in the world, now days India is also threatened by one problem *i.e.*, the growing number of vehicles on the Indian roads and inadequate capacity to accommodate the traffic. Heavy traffic congestion and endless list of highway accidents fuelled the motivation to increase driver comfort, safety and convenience. So, well-designed and logically controlled automated system will certainly lead to reduction in road accidents. As braking is frequently applied while driving, therefore, effort must be made to reduce the stopping distance as less as possible. One of such system is Antilock Braking System (ABS). ABS holds and releases the brake pressure according to some predefined logic and prevents wheel lockage and thus leads to shorter stopping distance and better steerability. Effect of camber and fork angle on ABS is considered here.

1.1.1 Vehicle Dynamics

Vehicle dynamics is a branch of science which deals with the study of response of vehicle in various in-motion situations. It includes the prediction as well as calculation of the effect of various forces and moments on the vehicle. It includes lateral vehicle dynamics, longitudinal vehicle dynamics, steering control, automotive suspension, fuel economy and vehicle emission.

For any vehicle, the forces and moments acting on each wheel of the vehicle have higher influence on the dynamics of the vehicle. Due to the vertical load of the vehicle, the surface contact of the tyre with the ground is called contact patch. All the tyre forces and moments are assumed to be at the centre of the contact patch. Mainly, longitudinal tyre force (F_x), lateral tyre force (F_y) and self-aligning moment (M_z) are considered for the dynamic analysis of the vehicle. Some other important forces are aerodynamic drag force (F_d) and rolling resistance (R_x) of the tyre.

The Longitudinal tyre force (F_x) depends on the slip ratio, normal load on the tyre and the friction coefficient of the tyre-road interface. Part of the normal load comes from the weight of the vehicle and the remaining part is influenced by the fore-aft moment of the centroid of the vehicle during braking and acceleration. This slip ratio (σ_x) is defined as the ratio of difference between the angular velocity $(\dot{\theta}_{ty} r_t)$ and longitudinal vehicle velocity $(\dot{x})$ of tyre to the linear speed of the vehicle and longitudinal slip ratio during acceleration is expressed as

$$\sigma_x = \frac{\dot{\theta}_{ty} r_t - \dot{x}}{\dot{\theta}_{ty} r_t} \tag{1.1}$$

For a driving wheel, $\dot{\theta}_{ty} r_t > \dot{x}$ so, the net velocity of the tread is the direction opposite to that of longitudinal velocity. There is a region in the contact patch where there is no sliding motion with respect to the ground. This region is called the static region. As the tyre enters this region, the top of the tread element moves with the velocity $\dot{\theta}_{ty} r_t > \dot{x}$. Hence, the tread element bends forward. This bending deflection is proportional to the slip velocity *i.e.*, $\dot{\theta}_{ty} r_t > \dot{x}$ and the time duration for which the tread element remains in the contact patch. Since the time duration is inversely proportional to angular velocity of the tyre $(\dot{\theta}_{ty} r_t)$. Hence the bending deflection or the longitudinal force is proportional to slip ratio σ_x.

The lateral tyre force (F_y) is proportional the slip angle of the tyre. The slip angle (β) of the tyre is defined as the angle between the orientation of the tyre (δ) and the orientation of the velocity vector of the wheel (θ_v) as shown in Fig. 1.1.

Therefore slip angle is $\beta = \delta - \theta_v$. In the static region of the contact patch, there is no lateral displacement. If the velocity of the wheel is V, the lateral component of the velocity is $V \sin\beta$, therefore, the magnitude of the lateral deflection is proportional to the lateral velocity and time taken by the tyre in the contact patch. Since the lateral velocity is proportional to velocity and slip angle while the time spent is proportional to rotational velocity, therefore, lateral force is effectively proportional only to slip angle.

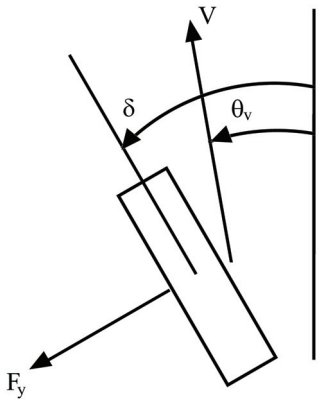

Fig. 1.1 Tyre slip angle and lateral force

Some sophisticated models are also created to calculate the longitudinal tyre force (F_x), lateral tyre force (F_y) and self-aligning moment (M_z). The Pacejka's magic formula tyre model calculate the longitudinal force, lateral force and self-aligning moment for wide range of slip ratio and slip angle. The force generated (y) is expressed as the function of input variable (x) as follow:

$$y(x) = D\sin[C\tan^{-1}\{Bx - E(Bx - \tan^{-1} Bx)\}] \tag{1.2}$$

Where, output variables (y) are: (F_x), (F_y) and (M_z) and input variables (x) are: (σ_x) and (σ_y).

The model parameter B accounts for stiffness factor, C accounts for shape factor, D accounts for peak value and E accounts for curvature factor.

Some other forces are aerodynamic drag force (F_d) which is given as

$$F_d = \frac{1}{2}\rho C_d A_F (V_x + V_{wind})^2 \tag{1.3}$$

where (ρ) is the mass density, (C_d) is the aerodynamic drag coefficient, (A_F) is the frontal area of the vehicle, (V_x) is the longitudinal vehicle velocity and (V_{wind}) is the wind velocity.

Another force is the rolling resistance (R_x). Due to normal loads of the vehicle, the tyre is deflected as it goes through the contact patch and then comes back to its original shape after passing through the contact patch. The energy absorbed

during deformation is not completely recovered on regaining its original shape. Therefore, the normal load (F_z) is not symmetric and is more during first half of contact patch. Hence it is said that the normal load is displaced by distance (dx) as shown in Fig. 1.2.

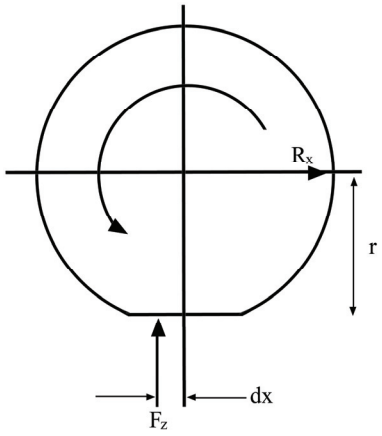

Fig. 1.2 Schematic representation of rolling resistance

The moment $(F_z dx)$ due to the offset of normal load is balanced by rolling resistance force $(R_x r)$. Hence rolling resistance is given as

$$R_x = \frac{F_z dx}{r} \tag{1.4}$$

1.1.2 Bond Graph

Nowadays, no one wants to waste money in doing experimental testing's on physical systems. As number of simulation software's are available in the market which are very inexpensive ways to model and analyse different physical systems. One of such technique is Bond Graph modelling developed by H.M. Paynter. Once the basic governing mechanism of any physical system is clear, its bond graph can be prepared very easily and the rest of the information can be derived from the bond graph itself. Thus bond graph portraits the exact physical structure of the system. Bond graph is a common tool to model systems lies in different energy domains.

Every system flow energy within itself and with surrounding. This energy flow in bond graph is done through bonds. In bond graph, a modeller can break the system into basic entities and once the modelling of the individual sub-system is done, these sub-systems are put back to get the main system. In bond graph, the

basic elements are inertances, compliances and resistors. External sources are named as source of effort and source of flow.

1.1.3 Antilock Braking System

Antilock braking system (ABS) is originally developed to prevent locking of wheels during hard braking. But nowadays, it also applies the braking torque in such a fashion that the slip ratio does not exceed the threshold values. Modern ABS is equipped with speed sensors provided at each wheel which will identify the locking of wheels; controller which receives the information from the speed sensors and generate the corrective signals; valves which applies, hold or release the brake pressure from the master cylinder to the brake callipers and last is pump which put back the brake pressure in the lines once it is released by the valves.

The basic objective of the ABS is to hold or release the brake pressure according to some logic, to prevent skidding of wheels. The ABS can be classified according to number of channels and number of sensors. Number of channels is the number of valves in the pressure line. Four-channel, four-sensor ABS consists of speed sensors for all the four wheels and valves for all the four wheels. So, all the four wheels are controlled individually by the controller. Three-channel, four-sensor ABS consists of sensors for all the four wheels, individual valves for the front wheels, but only one valve for the rear wheels. Three-channel, three-sensor ABS are commonly found in pick-up trucks with individual sensors and valves for the front wheels, but only one common valve and sensor for rear wheels. One-channel, one-sensor ABS is found with pick-up trucks with rear ABS. It has one sensor and one valve for the rear axle.

A major problem in ABS is the prediction of threshold values of slip ratio. The process of determining whether wheels are going to lock is called prediction and the slip ratio at this point is called the prediction point slip. The process of determining whether or not the danger of locking is passed is called reselection and the slip ratio at this point is called reselection point slip.

Different logic based controllers are there based on different algorithms. But the basic motto is same of all the controllers-that is, to prevent skidding. Any controller unit should not fail to indicate the wheel lockage, false prediction of the lockage of the wheel and maintain slip ratios between threshold values.

1.2 CONTRIBUTION OF THESIS

- Effect of camber angle and fork angle on the stopping distance and turning radius is stated.
- Effect of camber angle and fork angle on the longitudinal speed of the vehicle is stated.
- For fixed steering angle, relationship between camber angle and fork angle is stated.
- Stability of the vehicle is studied with ABS while maneuvering, for particular value of camber and fork angle.
- Variable camber angle mechanism is modelled with the help of quarter car model.
- Steering effect of camber angle is seen in four wheel vehicle model
- Control algorithm for antilock braking system for maintaining slip ratio between 0.2–0.25.

1.3 ORGANIZATION OF THESIS

This thesis comprises of six chapters. The overview of the theses chapters is given below for a clear and concise idea of the research. Chapter 1 explains some basic concepts of vehicle dynamics, bond graph and antilock braking system. These concepts are going to be used in the entire thesis.

In order to get a good grasp of the on-going research and latest technology, Chapter 2 is given to literature review. All the information is written in nut shell. The literature pertaining to bond graph, antilock braking system and camber and fork angle is discussed. From the literature survey the objective of the present thesis is discussed.

Chapter 3 deals with the basic concepts of bond graph modelling. Brief understanding of the basic concepts are discussed for the modelling of systems lies in different energy domains. The design of braking system is done. The bond graph model is constructed. The kinematic equations for bicycle vehicle model are derived which includes the effect of camber and fork angle. The major part of the bond graph of bicycle model is based on these equations. Effect of camber and fork angle on stopping distance and turning radius is studied.

Variable camber mechanism attached with steering system is designed and simulated in chapter 4. The bond graph of quarter car model is constructed to analyse the mechanism. While taking a left turn the mechanism gives positive camber angle to the left front wheel.

Bond graph of four wheel model of the vehicle body and subcomponents are made chapter 5. Steering effect of camber angle is seen from chapter. Also vehicle moves in circular path and with fixed speed for constant steering angle. The controller applies the brake torque such that the slip ratio is always in between 0.2–0.25.

Chapter 6 is for conclusion. The results are given chapter wise. Based on the research, the areas where work can be done are stated for future exploration.

CHAPTER 2

LITERATURE REVIEW

2.1 INTRODUCTION

In the past few decades antilock braking systems and several different types of controller have been mounted in different vehicles for increasing the vehicle safety and stability. Different controllers are based on the measurement of different parameters like tyre-road friction coefficient, slip threshold, wheel deceleration and reference vehicle speed. Antilock braking system is a complex system having components lies in several energy domains. Bond graph approach is well suited for modelling of systems lies in different energy domains. Camber and fork angle plays an important role in vehicle stability and steerability.

2.2 BOND GRAPH MODELLING

Bond graph represents the paths of exchange of energy within a system-structure. Bond graph technique is comparatively easier in modelling of systems consisting of several sub-systems which are residing in different energy domains and formulation of system equations need not be required at first stage for bond graph modelling and these equations are generated automatically by any standard bond graph software. Bond graph modelling is a unified approach in modelling and simulation of physical systems lying in different energy domains [**1–2**]. One can interpret the energy interactions between different parts of the model and can correct the computational problems by making necessary changes in the model. Bond graph approach is extensively used to study the dynamic response of the vehicle [**3**]. A four wheel model with electrically controlled brakes and steering were developed to study the dynamic response of the vehicle [**4**]. The engine model along with drive train and vehicle dynamic models with complexity were developed in [**5**].

Note that bond graph is not a numerical solution tool; it is a representation of the system-structure. A bond graph gives equations of motion with static and dynamic constraints, but does not directly give its numerical solution. One has to use normal numerical techniques to perform computational work. These

equations can be used to other modelling technique like Simulink in MATLAB. The representation of lumped parameters and constraints in a bond graph model expose the structure of the model. One can see the physical connections from the model structure and interpret the energetic interactions between the components of the model. At the same time, one can see the structure of the resulting equations of motion and foresee the computational problems and thereby make necessary changes to the model or the so-called conceptual prototype. That is why a bond graph model lies somewhere between the physical system description and its mathematical description in final differential algebraic equations form.

Bond graph modelling is ideally suitable for designing mechatronic systems [**6–7**]. Moreover, they have been recently used for various hardware-in-the-loop simulations and virtual reality applications [**8–9**]. Bond graph representation of multibody systems with kinematic loops has been developed in [**10**]. Other applications of bond graph modelling in mechatronic systems relate to estimation [**11–12**], identification [**13**], fault detection [**14–16**] *etc*.

2.3 ANTILOCK BRAKING SYSTEM

The heart of any antilock braking system is its governing algorithm according to which it continuously releases the break pressure and later reapplies it again when condition of wheel lock-up is passed. The maximum value of adhesion between the tyre and road does not occur at a fixed value of slip ratio, but it lies within the range depending on the friction coefficient and vertical load. The detailed literature review of antilock braking system is presented here.

A number of functional tests on Virtual Car (VC) in a Rapid Control Prototyping environment (RCP) were performed in [**17**]. ABS algorithm had been done in Matlab/Simulink. The algorithm was tested by Software In the Loop (SIL) co-simulation with 20-sim (version 2.03), a vehicle dynamic simulation model and a Simulink model of hydraulic circuit. The Slip Control Strategy (SCS) controls the slip independently of all the four wheels. The SCS keeps the slip in between the calculated threshold values. The Electronic brake distribution (EBD), compensates the front-rear load transfer while braking, by limiting the brake cylinder pressure on the rear axle. The Wheel Deceleration ABS Activation

(WDAA) algorithms identify any instability in the wheel and activate any suitable action even when slip threshold is not reached.

A number of functional tests in the RCP environment were done. The simulator was a multiprocessor system; the entire vehicle was splits into three functional parts: the vehicle dynamic real-time simulator, the power train real-time simulator and the body electronic simulator. It concluded that the internal wheels has higher tendency to lock, so ABS reduces the brake cylinder pressure on internal wheels. On low coefficient of friction (μ), the mean pressure on the front and rear axle were almost same because of small load transfer. On high coefficient of friction (μ), because of large transfer, the mean pressure of rear axle should be kept significantly lower as compared to front axle.

The dependence of deceleration on primary speed for vehicles with ABS and without ABS was studied in [**18**]. Deceleration of the vehicle without ABS on dry road of asphalt surface decreases with increase in primary speed whereas deceleration increases with increase in primary speed for vehicles with ABS. The time of deceleration and the time of disbraking were usually less for vehicle with ABS as compared to those without ABS on dry road of asphalt surface. In winter condition, the vehicles without ABS were held up on a snow-covered surface of the road more efficiently because the blocked wheels push and thicken the road in front of them. The wheels of vehicle with ABS remain un-blocked and did not contact with the wet surface of asphalt road and hence, deceleration was smaller. However, ABS has one significant positive advantage as there is possibility of driving the vehicle.

The braking of motorcycle while maneuvering a curved path with camber or steering angle was studied in [**19**]. Motorcycle requires large camber and small steering angle for maneuvering a curved path. Whereas, four wheel vehicle requires small camber and large steering angle. ABS hydraulic modulator was used to control the brake pressure. It contains a spool which is driven by motor and moves vertically and thus, restricts the piston movement. When the driver applies the brakes, high pressure oil supply is connected to the chamber and enters the brake callipers. If the wheels are going to lock, the motor driven spool moves upward. Therefore, piston was pushed upward by the oil pressure and thus it restricts the high pressure oil supply to the chamber. Also, upward movement

of the piston increases the volume inside the chamber and thus, reduces pressure in the chamber as well as in the brake calliper connected to the chamber. An ABS controller which uses camber angle and lateral acceleration to control brake pressure, was used here [**19**]. A fuzzy sliding controller was used so that oil pressure in the callipers always follows the reference pressure.

An ABS controller using bond graph was designed in [**20**] and then it is applied to different vehicle dynamics model like bicycle and four wheel model. In this ABS algorithm, brake torque was varied in accordance with the shifting of longitudinal slip ratio between maximum and minimum value. Thus slip ratio is maintained in a particular range called sweet-spot in order to have better stability and steerability. The longitudinal force was dependent on longitudinal slip ratio whereas, the lateral force and self aligning moment depends on vertical load and lateral slip angle. These are calculated by Burckhardt's formula. Four wheel models were developed to study the effect of load transfer during braking. Load transfer was from rear axle to front axle while braking and vice versa for accelerating. Also, load transfer was from inner wheels to outer wheels while maneuvering a curved path. Tests were conducted on different road conditions.

The combined regenerative and antilock braking system was studied in [**21**]. The regenerative braking algorithm distributes the brake force depending on various parameters. If the regenerative braking force was less than the required maximum braking force, both regenerative as well as ABS will work together and if regenerative braking force was more than the required braking force, only regenerative braking was applied. During regenerative braking, vehicle uses the motor as the generator to charge the regenerative battery which will provide the extra torque during acceleration. Continuously Variable Transmission (CVT) was used to maintain generator input speed constant during regeneration. The variation of CVT with load transfer was much steeper as compared to without load transfer. Sliding Motion Controller (SMC) was used to keep the slip ratio in predefined range. Regenerative SMC based ABS was also analysed for four wheel vehicle.

In conventional ABS, brake pressure was applied and released only to prevent wheel lock-up [**22**]. This procedure wastes lot of compressed air. A slip control makes only small adjustments to keep the wheels in optimum slip point

and thus reduces the compressed air consumption. This leads to small air storage system and energy used to compress air. A gain-scheduled slip controller was developed. The controller was designed to ensure satisfactory gain for each speed. Therefore, the controller switches between these predetermined gain values according to vehicle speed. Due to sluggish response of ABS valves, a new fast acting braking actuator was designed. The binary-actuated valves operate in either fully open or fully closed states, with permanent magnets holding each valve in a given state. A short electrical pulse alters the magnetic field, causing the valve seat to snap to the opposing state, with the help of a mechanical spring.

A sliding mode PMW slip-ratio controller was developed in [**23**]. According to the decision algorithm of the PMW sliding motion controller, 1 means electric motor was remained in the compressed process and -1 means that electric motor was maintained in the decompressed process. The controller signal varies between -1 to 1, therefore, rotation of the electric motor was not continuous. The rotating time was proportional to the absolute value of the signal. The PMW controller uses the P-R conditions consists of four prediction and eight reselection conditions. If P condition was satisfied, the wheel was tending to be locked and ABS releases the brake pressure. If R condition was satisfied, the danger of wheel lockup was averted and brake pressure can be applied.

The control logic for ABS based on the measurement of longitudinal forces was developed in [**24**]. Since, deceleration was not related only to the tyre performance and slip was not measured but was computed by using estimated longitudinal velocity of the vehicle. Thus, deceleration and slip calculation are subjected to error. This control logic was independent of the measurement of tyre-road friction coefficient. To set the two thresholds, condition of maximum value of deceleration and maximum value of slip were used.

The improvement in the performance of ABS due to the information provided by the smart tyres was studied in [**25**]. Smart tyres provide real-time estimation of tyre-road contact forces and friction coefficient. Smart tyres contain accelerometers which calculate the circumferential and radial acceleration during passage of the accelerometer from the contact patch of the tyre. The signals of the accelerometer were affected by the footprint area, the longitudinal, lateral and

vertical load of the tyre, rolling speed and maximum available friction coefficient.

The concept of limit braking for motorcycles, in which peak torque was attained in 0.25 s was studied in [**26**]. Slipper clutch disengaged the rear wheel from the engine when throttle was closed. Otherwise, brake torque was sufficient to lock the rear wheel. High-bandwidth Proportional Integral Differential (PID) slip-tracking controllers were used. Parameters of the braking control scheme were optimized to get minimal final speed.

The condition of dampers and suspension affects the vehicle handling and driving-safety significantly [**27**]. Worn bushes increase the clearance in the entire suspension system leads to inadequate damping and inaccurate wheel guidance. The brake force on the tyres with vehicle equipped with ABS with defected and new dampers is studied. The wheel with defected damper loses the contact with the road twice. The directional stability of the vehicle is badly affected by the worn bushes.

The effect of transient load shifting due to cargo movement on ABS performance was studied in [**28**]. Analytical and empirical mathematical models were presented to describe the chassis, tire-road interface, wheel, brake modulator, and cargo dynamics. Two strategies, a model-free table lookup and model-based discrete nonlinear controller, were presented to regulate the ABS modulator's operation. These vehicle and controller dynamics had been integrated into a simulation tool to investigate the effect of transient weight transfers on the vehicle's overall stopping distance and time. Representative numerical results were presented and discussed to quantify the ABS systems' performance for various loading and operating conditions.

2.4 CAMBER AND FORK ANGLE

Camber angle has a strong effect on vehicle dynamics. Camber angle provides the necessary lateral force which is required for cornering. Camber angle is more important for two wheelers while cornering as compared to four wheel drive. Fork angle plays a crucial role at high speed stability of the vehicle.

The characteristics of the motorcycle with added camber angle to the front frame for two different steering conditions was investigated [**29**]. One with

constant steering angle and constant camber angle and another was free steering angle and constant camber angle. The front frame can camber with respect to the rear frame moving through an angle about the horizontal axes. The cambering of the front frame has a similar effect as of steering angle input but with less sensitivity. Cambering has no effect on the rolling response of the vehicle. Influence of cambering of the front frame in free control is similar but opposite to that of fixed control steering.

The steady state turning of the bicycle to measure steering torque, steering angle, bicycle, acceleration and angular velocity was studied [**30**]. 134 trials were taken on nine different radii and three speeds and three rider lean conditions. Torque sensor within the steering tube measures the torque transmitted between the handle bars and the front wheel. Optical encoder was used to measure the steering angle which was attached to the bicycle fork. Bicycle speed is calculated by dividing the circumference of the front wheel with time required to complete one revolution. Acceleration and angular velocity were measured by three-axes accelerometer and single-axes angular rate gyros. It was demonstrated that the lateral shift of the bicycle-rider centre of mass strongly influences the steering torque. Whereas, steering angle is largely insensitive to rider lean. This proves that steering angle is better parameter to consider as compared to steering torque.

Extreme cornering leads to rollover accidents, was studied [**31**]. The effect of camber angle on overturning moment was studied. Camber angle is considered as the lateral slip input of the model. Tyre camber angle has great influence on the overturning moment of the vehicle. Vehicle fishhook simulation was done for different tyre model to investigate the effect of camber angle on vehicle dynamics.

Some important issues connected with wheel slip due to spin were clarified [**32**]. The spin velocity was defined as the component of the rotational velocity of a rolling body normal to the contacting surface. For a tyre, two possible components of spin: camber and turning were distinguished. Different from a homogeneous rolling body, the tyre with its peculiar structure may give quantitatively different responses to each of these components. When comparing the steady-state responses with side-slip and with pure turn slip (path curvature)

of some analytical tyre models, it turns out that the aligning torque stiffness was equal to the turn-slip side-force stiffness.

The lateral force of a tyre is a function of the sideslip and camber angles [**33**]. The camber angle has a significant effect on the stability of a vehicle by adjusting the required lateral force. To control the camber angle, we can use the caster angle of the wheel. We introduce a possible variable and controllable caster angle in order to adjust the camber angle when the sideslip angle cannot be changed. As long as the left and right wheels are steering together according to a kinematic condition, such as Ackerman, the sideslip angle of the inner wheel cannot be increased to alter the reduced lateral force because of weight transfer and reduction of the normal load. A variable caster mechanism can adjust the camber angle of the wheels to maximise the lateral force, when needed.

LuGre model describes the three-dimensional tyre friction dynamics [**34**]. The model has a three-state lumped-parameter form and an analytical solution for tyre static curves. It is simplified using the assumption of a constant slip speed along the contact patch length. Two approaches to the introduction of a variable-slip-speed effect are considered. The first is based on stepwise approximation of the slip speed along the contact patch length, and the second includes a specific, spatially distributed additive deflection term. Both approaches preserve the three-state lumped-parameter model form and an analytical steady-state solution.

An analytical approach for estimating the longitudinal and the lateral adhesive coefficients between the tyre and the road surface through the Pacejka's magic formula tyre model for both pure-slip and combined-slip conditions, were derived [**35**]. The relationship between the vehicle velocity and the parameters of the Pacejka's magic formula tyre model was discussed in the study. One may analyse the adhesive coefficient through genetic algorithm identification to search for the parameters of the Pacejka's magic formula tyre model from experimental data. A test stand was set up for adhesive force experiments. Only brake slip was studied in the experiments.

The steady-state cornering test using a sport-touring motorcycle was performed in [**36**]. The measurement data from this test includes tyre force, tyre moment, and tyre slip angle that have not been practically addressed in the research of motorcycles, in addition to normal measurement results for velocity,

steering angle, steering torque, roll angle *etc*. There was a strong relationship between the motorcycle dynamics characteristics and the tyre slip angle. Measurements were taken not only the with normal rider's lean angle, but also measurements in the case where the rider's lean angle was intentionally changed, in order to investigate the effects that a change in the rider's posture has on the variation in the measurement results of the motorcycle's dynamics.

The effect of giving negative camber angle to the rear wheels of the wheel chair was studied in [**37**]. Camber is known to affect the variables such as rolling resistance, the wheel chair downhill turning moment on lateral slopes, the life of the rear wheel ball bearing. The relation between the heights of the rear axle with camber angle has quadratic relation. With positive castor angle, the external ends of the rear axle moved downward. With negative camber angle, it first increases, reaches a plateau and then decreases. The track width was a inverse function of camber angle. Negative camber angle brings the centroid nearer to the rear wheels.

The side slip and camber characteristics, like the forces and moments generated as it rolls forward under different circumstances were measured [**38**]. It required holding the vehicle at fixed orientation−that is, fixed camber angle and steering angle. It includes a cart that holds the bicycle wheel in the desired orientation, allows it to roll forward, applies a vertical load and measures the lateral force that develops between the tyre contact patch and fixed vertical surface.

2.5 OBJECTIVE OF THE PRESENT WORK

In most studies, braking of vehicle in a straight path has been considered. When vehicle moves in a curved path, the effect of camber angle and fork angle should be considered. The variable camber angle assists braking in a curved road but the turning radius of vehicle changes due to varying camber angle and fork angle. The bond graph model of bicycle vehicle is to be developed to study the effect of camber angle and fork angle on the performance of ABS when it manoeuvres a curved path. Variable camber mechanism is to be designed and analysed by using quarter car model and at the end, four-wheel model is used to study the effect in dynamic environment.

CHAPTER 3

PERFORMANCE OF ANTILOCK BRAKING SYSTEM FOR A BICYCLE VEHICLE MODEL

3.1 INTRODUCTION

Antilock braking system (ABS) is now-a-days is very much common in vehicles as it increases vehicle's safety and steerability. When brakes are applied to a vehicle with ABS, while maneuvering a curved path, the camber angle increases the contact patch of the tyre with the ground up to a certain extent and thus it assists braking. Camber angle can be either positive or negative. When the top of the tyre is tilted outward, it has positive camber angle and when the top of the tyre is tilted inward, it has negative camber angle. Two wheelers always have positive camber angle either they are maneuvering left or right. Two wheelers require large camber angle and small steering angle while turning to reduce the road traversed by them.

The vehicle should have small turning radius while maneuvering a curved path. So fork angle should be such that it increases the stability of the vehicle at higher speed and also has small turning radius. If the line drawn through the steering axis meets the road surface slightly ahead of the contact point of the tyre with the ground, it has positive fork angle and if it meets behind the contact point of the tyre with the ground, it has negative fork angle.

Antilock braking system (ABS) maintains the slip ratio in such a range, according to road condition, maximum frictional resistance can be achieved. In this way ABS decreases the braking distance. It uses an on-off control strategy to prevent locking of wheels and thus preventing skidding of the vehicle. Thus, ABS increases the directional stability and steerability while braking. Friction force between road and tyres during braking is a non-linear function of slip ratio. Different ABS controllers have been developed to achieve highest coefficient of friction between the road-wheel interface. The main limitation of conventional ABS is that slip ratio is always maintained in a particular range (sweet spot zone) for any type road condition (snow, wet or dry condition) rather than optimal value.

3.2 BOND GRAPH MODELLING

Bond graph is a graphical modelling tool which represents power exchanges between different dynamical parts in a system. It provides a physical insight into the dynamic behaviour of a system. The notation of causality provides a tool not only for formulation of system equations but also for qualitative analysis of the system behaviour, *viz*. controllability, observability, fault diagnosis, *etc*. With the help of bond graph approach, a physical system can be represented by symbols and lines, identifying the power flow paths.

3.2.1 Equal flow junction and equal effort junction

A simple circuit with a resistor, a capacitor, an inductor and a power source all connected in series is shown in Fig. 3.1(a). The transmission of power from the source is represented by a line connected to an element SE. SE represent source of generalised effort. The line leading to the various elements are abstract representation of paths of power and are called bonds as shown in Fig. 3.1(b). Each of these bonds is associated with two power variables, generalised effort and generalised flow. The constraint imposed by the circuit is such that the flow (current) are equalised in the bonds.

$$f1 = f2 = f3 = f4 \tag{3.1}$$

The constraint of equalisation of the flows is represented by inserting an icon 1 at the junction point. 1 junction is an abstract representation of the constraint of equation of flow along the bonds connected to it.

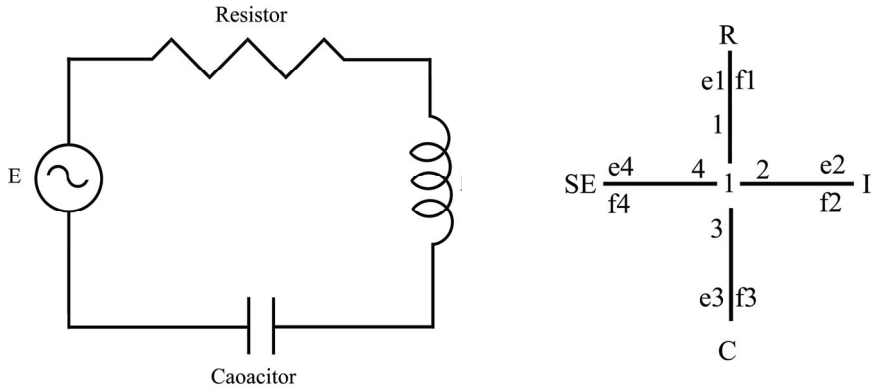

Fig. 3.1 (a) A series electrical circuit and (b) its basic bond graph

Similarly, Fig. 3.2(a) shows the circuit which imposed the constraint such that effort (voltage) is equal in the bonds.

$$e1 = e2 = e3 = e4 \tag{3.2}$$

The constraint of equalisation of effort is represented by inserting an icon 0 at the junction point. Therefore, 0–junction is the abstract representation of the constraint of equality of effort along the bonds connected to it (Fig. 3.2(b)).

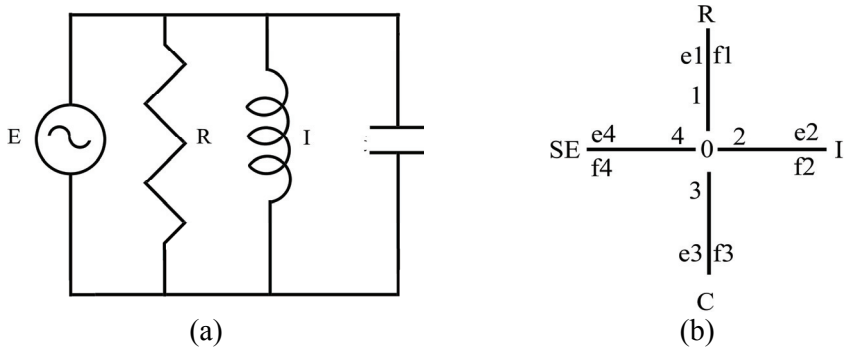

Fig. 3.2(a) a parallel electrical circuit and (b) its bond graph

3.2.2 Reference power direction of bonds

Bondgraph is the physical representation of the general system. The left and right, up and down, clockwise and anticlockwise are of no relevance. Therefore, a general view point should be created from which any particular system interpretation should be easily conducted. This is done by assigning reference power direction to the bonds. If J stands for junction and E stands for element, the half arrow represents the reference power direction as shown in Fig. 3.3.

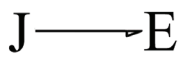

Fig. 3.3 Power direction of the bond

3.2.3 Single port bond graph elements with causality

In bond graph modelling, the inter connection takes place through abstract entities called energy ports. Each energy port is represented by a bond having associated with two factors of power (flow and effort). It is observed that the elements which have two terminals but single variable of energy associated with them, have, in bond graph single bonds attached to them.

Bond graphs have a notion of causality, indicating which side of a bond determines the instantaneous effort and which determines the instantaneous flow. In formulating the dynamic equations that describe the system, causality defines, for each modelling element, which variable is dependent and which is independent. By propagating the causation graphically from one modelling element to the other, analysis of large-scale models becomes easier. In bond graph notation, a causal stroke may be added to one end of the power bond to indicate that the opposite end is defining the effort.

For capacitive element, $E = kq$, but $f = \frac{dq}{dt}$. Therefore, $e = k\int f dt$. Since, $\int (\text{cause}) dt$, flow is the cause in capacitance. Similarly for inductive element, $P = mf$, $e = \frac{dP}{dt}, dP = edt$. Therefore, $P = \int edt$. Thus, effort is the cause in inductive element. Figure 3.4 shows representation of capacitive and inductive element along with there causality.

(a) (b)

Fig. 3.4 Representation of (a) capacitive and (b) inductive element along with their causality

A resistor has no time-dependent behaviour. Voltage is applied and a flow instantly obtained; or, a flow is applied and a voltage instantly obtained; thus, a resistor can be at either end of a causal bond. Figure 3.5 shows representation of resistor element.

Fig. 3.5 Representation of resistive element along with its causality

3.2.4 Two port bond graph element

There are only two kinds of two port bond graph elements, namely Transformer and Gyrator. In the bond graph, transformer is represented as ideal electrical transformer, a mass less lever *etc*. The transformer does not create, store or destroy energy. It conserves power and transmits the factors of power with proper

scaling as defined by the transformer modulus. The oriented arc indicates the way the modulus is applied. The transformer is best explained by a mass less lever as shown in Fig. 3.6.

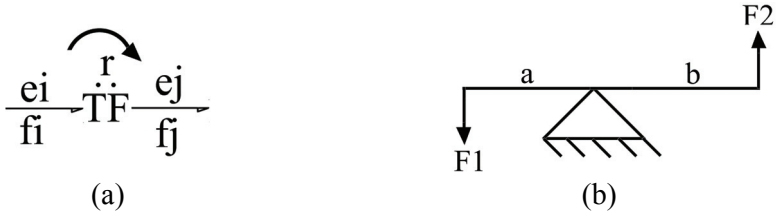

Fig. 3.6 (a) Representation of transformer element and (b) a mass less lever

From the geometry, it can be written as $F_2 = (a/b)F_1$ or $F_2 = rF_1$. Where, r is the module of the transformer. Often, transformer with variable modulii is presented as MTF.

The gyrators relate the relation between flow to effort and effort to flow. The simplified example of gyrator is gyroscope. Whenever flow belongs to any particular domain of energy is to the effort variable of the same or any other domain of energy, the bond graph element gyrator is used to represent such an action. Figure 3.7 shows representation of gyrator.

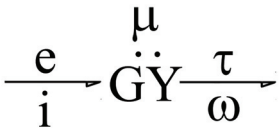

Fig. 3.7 Basic representation of gyrator

3.3 RELATIONSHIPS BETWEEN CAMBER AND FORK ANGLE

Many efforts have been made to increase the coefficient of friction between the tyre and the road while braking. Most important method is by adjusting the camber angle and fork angle of the vehicle. The expression of camber angle (ϕ) as a function of fork angle (λ) and steering angle (δ) is given as [**39**].

$$\cos\phi = \cos\delta \sin^2\lambda + \cos^2\lambda \tag{3.3}$$

From Eq. (3.3) it is clear that for a fixed steering angle *i.e.*, for a fixed turning radius of road, camber angle and fork angle are directly proportional to each other. Since camber angle and fork angle decides the area of contact patch

between the tyre and the road, their variation plays an important role in the vehicle stability and steer ability specially while manoeuvring a curved path. As today roads are very congested with vehicles, small turning radius is desired during lane changing and also during parking. Also, while manoeuvring, contact patch of the tyre with the road should be maximized so that braking of the vehicle is efficient. It will be shown that stopping distance after applying ABS decreases with the increase of positive camber angle reverse case happens and the for the castor angle.

3.4 MODELLING OF MECHANICAL ABS

Tyres are the points of contact of the vehicle with the road. Rather tyres do not make point contact, they deform due to the vehicle load and make a surface contact called contact patch. All tyre forces and moments are considered to act at the centre of the contact patch of the tyre. The Pacejka's magic formula may be used to calculate the longitudinal force, lateral force and self-aligning moment of the tyres [**40**].

3.4.1 Lateral and longitudinal tyre forces

Longitudinal slip ratio (σ) of the tyre is an important characteristic to find out whether wheels could be locked during braking. This slip ratio (σ_x) is the ratio of difference between the longitudinal vehicle velocity $(\dot{x})$ and angular velocity $(\dot{\theta}_{ty} r_t)$ of tyre to the linear speed of the vehicle and longitudinal slip ratio during braking is expressed as

$$\sigma_x = \frac{\dot{x} - \dot{\theta}_{ty} r_t}{\dot{x}} \tag{3.4}$$

Lateral slip ratio (σ_y) is the ratio of lateral velocity $(\dot{y})$ to the longitudinal velocity $(\dot{x})$ of the vehicle and it is given as

$$\sigma_y = \frac{\dot{y}}{\dot{x}} \tag{3.5}$$

According to the Pacejka's magic formula the force or moment generated (y) can be expressed as a function of input variable (x) as

$$y(x) = D\sin[C\tan^{-1}\{Bx - E(Bx - \tan^{-1}(bx))\}] \tag{3.6}$$

Where B is stiffness factor, C is shape factor, D is peak value and E is curvature factor and can be determined by measuring tyre forces and moments [**41**]. Output variable (y) can be longitudinal force (F_x), lateral force (F_y) and self-aligning moment (M_z) and input variable (x) can be either longitudinal slip ratio (σ_x) or lateral slip ratio (σ_y). Longitudinal force is generated due to longitudinal slip velocity $(\dot{x} - \dot{\theta}_{ty} r_t)$ and lateral force and self aligning moment are generated due to lateral slip velocity $(\dot{y})$ as there is no initial lateral velocity. The main drawback of Pacejka's magic formula is that it does not take into account the dependence of friction force on the velocity of the vehicle while braking. Though, this formula is a good one during motion of the vehicle at constant speed, this model is not used in this present work as velocity decreases during braking.

3.4.2 Design of braking system

Antilock braking system is a dynamic control system which prevents tyres from locking up during braking and provides maximum frictional force by maintaining slip ratio in an optimal range. If the value of slip ratio is high, it means angular velocity of the tyre is decreasing much faster, during braking, as compared to linear velocity of the vehicle. The grip of the tyre with the road is reduced and skidding of the vehicle may occur. Therefore, the brake torque is required to be reduced to increase the angular velocity of the tyre and thus the slip ratio reduces. At low values of slip ratio, the grip between the tyre and road again reduces. Therefore, the brake torque is varied such that slip ratio is maintained in a range bounded by maximum (σ_{max}) and minimum (σ_{min}) slip values.

The main parts of mechanical equivalent ABS are servo motor, lever arm, brake cable, return spring, brake rod, cam and brake shoe [**42**]. The voltage supply to the servo motor is controlled by ABS controller. One end of the lever arm is connected to the servo motor whereas other is connected to brake-rod which rotates the cam. The movement of cam expands and contracts the brake shoe. The return spring is used to come back to the initial position. The schema of ABS is shown in Fig. 3.8(a).

The calculation of friction force between the tyre and the road is very important in determining the amount of braking torque of the vehicle. Friction

model given by Burckhardt is used here to calculate the friction coefficient. It is given as

$$\mu(\sigma_x, \dot{x}_t) = [C_1(1 - e^{-C_2\sigma_x}) - C_3\sigma_x]e^{-C_4\sigma_x\dot{x}_t} \tag{3.7}$$

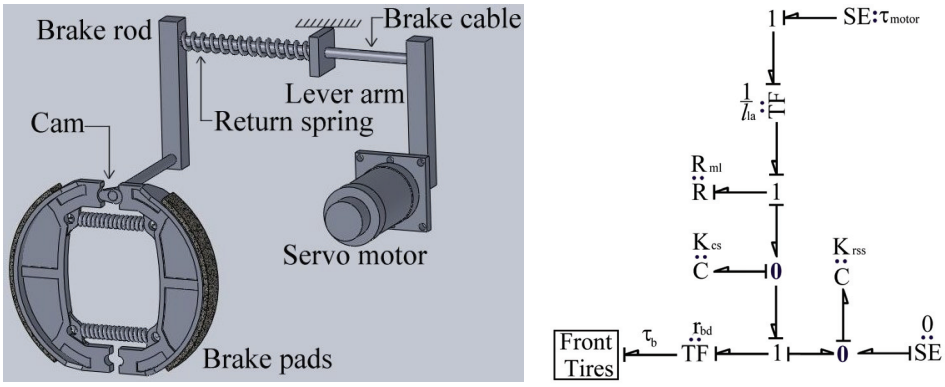

(a) (b)

Fig. 3.8 (a) Schema of mechanical equivalent ABS and (b) its bond graph model [**20**].

Where constant parameter C_1, C_2, C_3 and C_4 are determined experimentally for different road conditions. The values of these parameters for dry asphalt road surface which is very much common in Indian roads are given in Table 3.1.

Table 3.1: Tyre-road friction parameters [**43**]

Road surface	C_1	C_2	C_3	C_4
Asphalt, dry	1.029	17.16	0.523	0.03

The Burckhardt formula takes into account the velocity dependence of frictional force of the vehicle which is very important while designing any braking system. The relation between the braking torque (T) and longitudinal slip ratio (σ) is given below:

$$T_{i+1} = \begin{cases} 0 & \sigma > \sigma_{max} \\ T_i & \sigma_{min} \le \sigma \le \sigma_{max} \\ T_{max} & \sigma < \sigma_{min} \end{cases} \tag{3.8}$$

Braking torque should be zero if the value of slip ratio is greater than σ_{max} and maximum braking torque must be applied if slip ratio is less than σ_{min}. For all other cases same braking torque is applied as in last step. The optimal range of slip

ratio for which maximum frictional force can be obtained is 0.2–0.25 for all kind of road conditions [20].

3.4.3 Bond graph of braking system

The bond graph model of ABS is shown in Fig. 3.8(b). The controlled amount of voltage from the ABS controller is fed to the motor to produce torque (τ_{motor}) and is represented by the Se element. The mechanical losses are represented by the resistive element (R_{ml}). The cable stiffness (K_{cs}) is represented by the C-element. The return spring stiffness is K_{rss}. The other end of the return spring is connected to zero valued Se element which represents the ground. The output brake torque is applied to the bicycle vehicle model.

3.5 BICYCLE VEHICLE MODEL WITH CAMBER AND FORK ANGLE

A bicycle vehicle model is developed to study the effect of roll (ϕ), pitch (λ) and yaw (δ) motions on ABS while manoeuvrings a curved path. Schematic diagram of bicycle vehicle model is shown in Fig. 3.9 and its bond graph model is shown in Fig. 3.10.

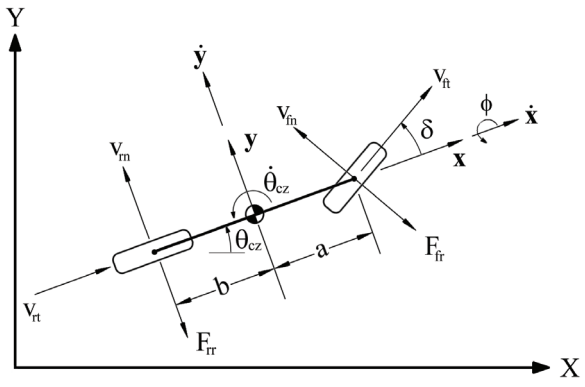

Fig. 3.9 Schema of bicycle vehicle model

3.5.1 Kinematic relations bicycle vehicle model and its bond graph model

The kinematic relations which are derived in [**20**] have been modified to study the effect of camber angle (ϕ) and fork angle (λ). Major part of the bond graph model of the vehicle has been constructed based on of these relations. Front

wheels are steered by an angle (δ). Normal and tangential component of velocity of the front tyres are given by

$$v_{\mathrm{fn}} = (\dot{y} + \dot{\theta}_{\mathrm{cz}} a)\cos\delta\cos\phi - \dot{x}\sin\delta\cos\lambda \tag{3.9}$$

$$v_{\mathrm{ft}} = (\dot{y} + \dot{\theta}_{\mathrm{cz}} a)\sin\delta\cos\phi + \dot{x}\cos\delta\cos\lambda \tag{3.10}$$

Similarly, normal and tangential component of velocity of the rear tyres are given by

$$v_{\mathrm{rn}} = (\dot{y} - \dot{\theta}_{\mathrm{cz}} b)\cos\phi \tag{3.11}$$

$$v_{\mathrm{rt}} = \dot{x} \tag{3.12}$$

Newton-Euler equations based on external forces, inertial forces and gyroscopic forces are given by

$$m_{\mathrm{vb}}\ddot{x} = m_{\mathrm{vb}}\dot{\theta}_{\mathrm{cz}}\dot{y} + \Sigma F_{\mathrm{x}} \tag{3.13}$$

$$m_{\mathrm{vb}}\ddot{y} = -m_{\mathrm{vb}}\dot{\theta}_{\mathrm{cz}}x + \Sigma F_{\mathrm{y}} \tag{3.14}$$

The bond graph of bicycle vehicle model has been constructed using Eq. (3.9–3.14) and is shown in Fig. 3.10. Torque from the electric traction motor (τ_{E}) is applied to the rear tyres whereas the braking torque (τ_{B}) from the ABS unit is applied to the front tyres. Power bonds are represented by half arrows, whereas information bonds are represented by full arrow. Vehicle inertial mass ($I : m_{\mathrm{vb}}$) and rotary inertia ($I : J_{\mathrm{vb}}$) is modelled at there respective 1-junctions which represent the linear and angular velocity of the centroid of the vehicle in the body fixed coordinate system.

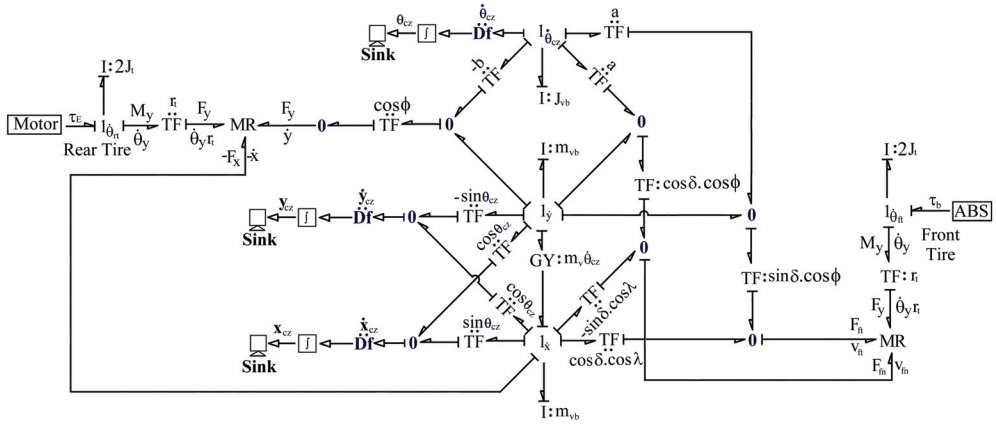

Fig. 3.10 Bond graph of bicycle vehicle model

The two modulated 3-port R-field (MR-elements) implement the Burckhardt formula. Tangential and normal components of the velocity are used to calculate the slip ratio by using Eq. (3.4–3.5). Therefore, Burckhardt formula (Eq. (3.7)) is used to calculate the coefficient of friction and hence to calculate the longitudinal and lateral tyre forces.

3.6 PARAMETER VALUES AND SIMULATION RESULTS

The parameter values used in the simulation is given in Table 3.2. The value of the constant parameters used in Burckhardt formula is taken from Table 3.1. The control logic based on Eq. (3.8) adjust the brake torque such that slip ratio always lies between 0.2–0.25. The road is considered as made of dry asphalt. The radius of the wheel is 0.3 m. The length of the vehicle is 2 m.

Table 3.2: Parameter values of bicycle vehicle model

Subsystem	Parameter values			
Vehicle body	$m_{vb} = 1000\ \text{kg}$	$J_{vb} = 100\ \text{kg m}^2$	$a = 1.0\ \text{m}$	$b = 1.0\ \text{m}$
Wheel	$J_t = 100\ \text{kg m}^2$	$r_t = 0.3\ \text{m}$		
	$C_1 = 1.029$	$C_2 = 17.16$	$C_3 = 0.523$	$C_4 = 0.03$
ABS	$\sigma_{max} = 0.25$	$\sigma_{min} = 0.2$		
Motor	$V = 100\ \text{V}$	$R = 0.1\Omega$	$\mu = 0.4\ \text{Nm/A}$	$G = 8$

All simulations are performed in SYMBOLS Shakti software [**44**]. It is an object oriented modelling and simulation technique which allows users to create models using bond graph. It automatically derives the reduced system equations from the bond graph model. The software has number of in-built as well as user made capsules of different basic engineering components. High level control analysis can also be performed using this software.

First, bond graph of the bicycle model is made in the bond pad and then simulation is done in symbols simulator. The parameters are properly considered and put in the simulator from Table 3.1 and Table 3.2. Then simulation is done for different values of the camber and fork angle. The practical range of camber angle (ϕ) is 0.2–0.5 rad. and that of fork angle (λ) is 0.3–0.8 rad. The value of

steering angle (δ) is kept fix to 0.1 rad. and is applied at t = 10 sec. ABS is applied to the front wheels of the bicycle model whereas rear wheels are motor driven.

3.6.1 Effect of camber angle without ABS

Figure 3.11(a) shows the variation of camber angle and for no fork angle while manoeuvring a curved path. It shows that the path traversed by the vehicle without camber angle which is a circle of diameter 52.22 m (base diameter). The diameter of the path is reduced by 61.35 cm if the camber angle of 0.2 rad. is considered and the path is reduced by 143.84 cm (with respect to base diameter) if the camber angle is 0.3 rad. Also, there is decrease in the longitudinal speed of 0.43 mm/s for 0.2 rad. and 1.03 mm/s for 0.3 rad. (which is shown in Fig. 3.11(b)) with respect to the speed of 10.81528 m/s which is the speed of the vehicle for without any camber angle. It is also observed from the Fig. 3.11(b) that the speed of the vehicle reduces due to the starting of the yaw motion of the vehicle at 10 s.

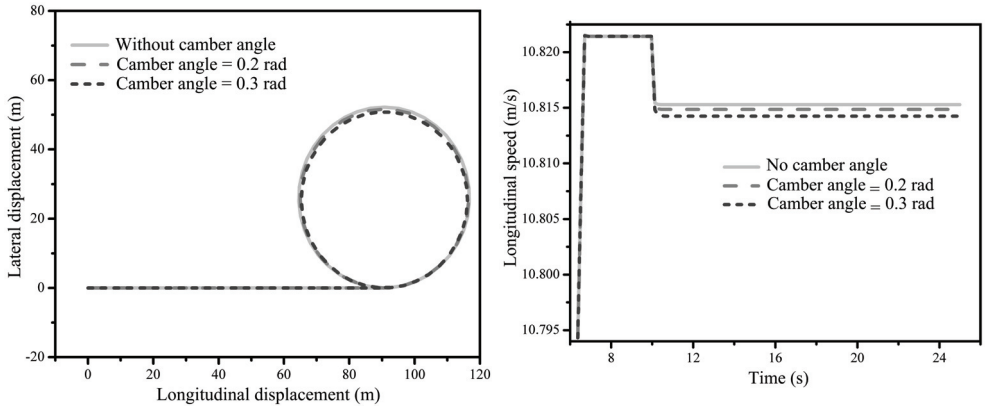

(a) (b)

Fig. 3.11 (a) Lateral displacement vs. longitudinal displacement of the centre of vehicle for different camber angles while manoeuvrings a curved path and (b) corresponding longitudinal speeds with no fork angle.

3.6.2 Effect of fork angle without ABS

Figure 3.12(a) shows that the path (thick grey line) traversed by the vehicle without fork angle is a circle of diameter 52.22 m (No camber and fork angle is provided to the wheel). The diameter of the circle is increased by 115.12 cm if the fork angle of wheel is 0.2 rad. and the path is increased by 264.4 cm with respect to the base diameter if the fork angle is 0.3 rad. Also, the longitudinal

speed is increased by 0.26 mm/s for 0.2 rad. and increased by 0.58 mm/s for 0.3 rad. (Fig. 3.12(b)) with respect to the base speed of 10.81528 m/s.

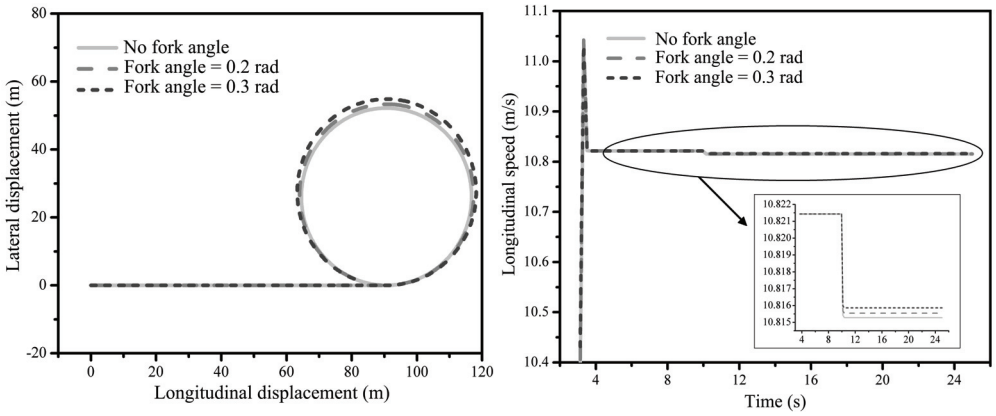

(a) (b)

Fig. 3.12 (a) Lateral displacement vs. longitudinal displacement of the centre of vehicle for different fork angles while manoeuvrings a curved path and (b) corresponding longitudinal speeds with no camber angle.

3.6.3 Effect of camber and fork angle on turning radius without ABS

Figure 3.13(a) shows the effect of camber angle on turning radius for different values of fork angle. It clearly shows that turning radius always decreases if we increase the camber angle. So camber angle is inversely proportional to the turning radius.

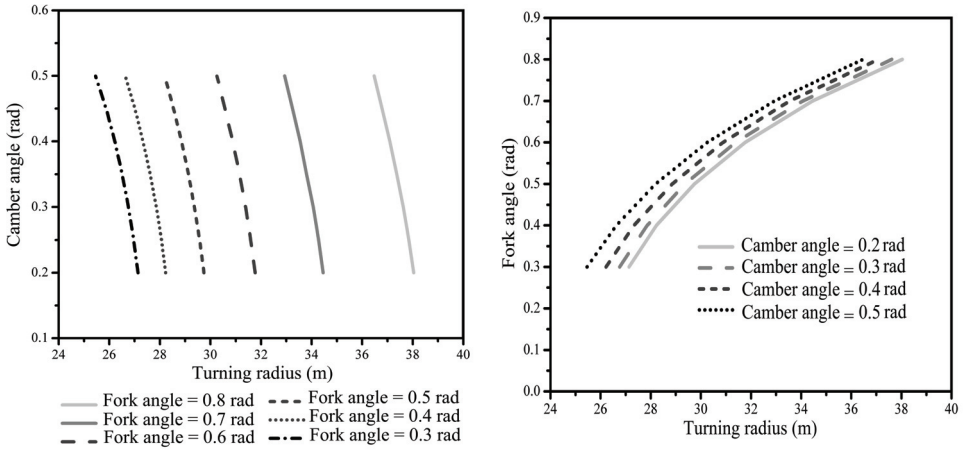

(a) (b)

Fig. 3.13 (a) Variation of camber angle with turning radius for different values of fork angle and (b) variation of castor angle with turning radius for different values of camber angle

Similarly, Fig. 3.13(b) shows the effect of fork angle on turning radius for different values of the camber angle. It also shows that turning radius always increases if we increase the fork angle. So fork angle is directly proportional to turning radius. Also for fixed turning radius, camber angle is proportional to fork angle as proposed in [**39**].

3.6.4 Effect of camber and fork angle individually on ABS

The effect of camber angle and fork angle on ABS is shown in Fig. 3.14. Initially the vehicle starts from rest and then it reaches at a speed of 33.6 km/hr at 8 s. At 10 s the vehicle is steered with a steering angle of 0.1 rad and the ABS is applied at 15 s to stop the vehicle. It takes 1.5 s after applying the brake to stop the vehicle. It is seen from Fig. 3.14(a), the vehicle exactly follows the path when ABS is applied with no camber angle. Figure 3.14(a) shows that, the stopping distance and turning radius both decrease with an increase in camber angle. So, increase in camber angle is advantageous during braking but it can not be increased after the specific limit (maximum limit of camber angle is 0.5 rad) as the path of contact between the tyre and the road again starts decreasing after that specific limit. Whereas, increase in fork angle decreases the stopping distance but it increases the turning radius while manoeuvrings a curved path (Fig 3.14(b)) but fork angle must be provided to the wheel to enhance the stability of the vehicle.

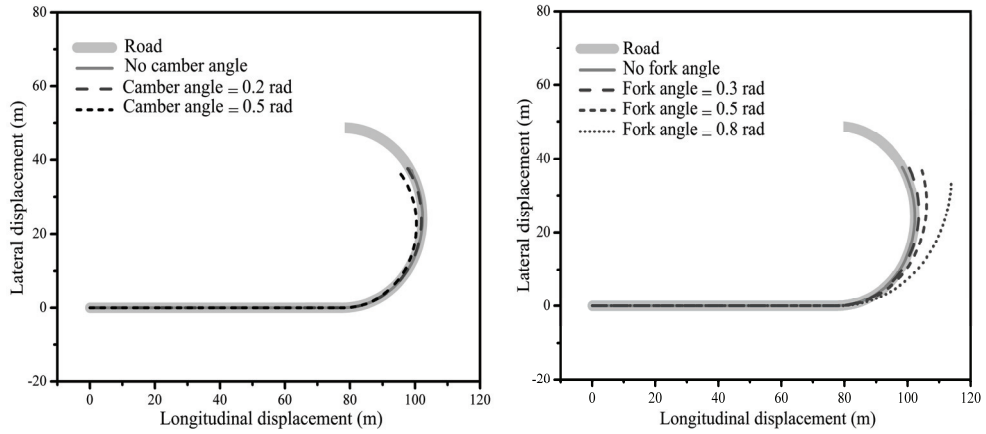

(a) (b)

Fig. 3.14 (a) Lateral displacement vs. longitudinal displacement of the centre of vehicle for different camber angles with no fork angle and (b) Lateral displacement vs. longitudinal displacement of the centre of vehicle for different castor angles with no camber angle

3.6.5 Effect of camber and fork angle for a fixed value of the other on ABS

Figure 3.15(a) shows the effect of camber angle while ABS is applied to the vehicle maneuvering a curved path for a fixed value of fork angle of 0.3 rad. The effect of fork angle while ABS is applied to the vehicle maneuvering a curved path for fixed value of camber angle 0.2 rad is shown in Fig. 3.15(b). It is concluded from Fig. 8, if the camber angle of 0.2 rad and fork angle of 0.3 rad is provided to the wheel, both stability of the vehicle can be enhanced as well as the vehicle follows the road. The slip ratio is maintained between 0.2 and 0.25 to obtain the maximum frictional force between the wheel and road and it is shown in Fig. 3.16(a). In Fig. 3.16(b), the vehicle speed and the corresponding speed of front wheel on which ABS is attached are shown. The angular speed of the front wheel is shown in inset during braking.

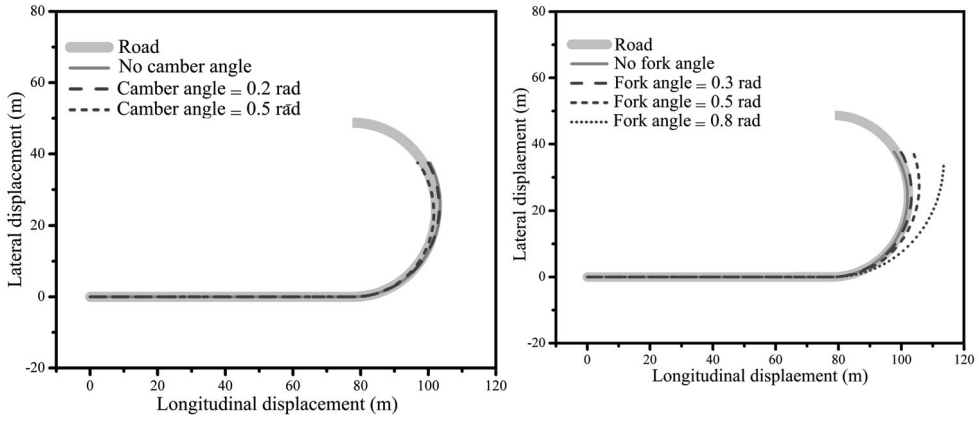

(a) (b)

Fig. 3.15 (a) Lateral displacement vs. longitudinal displacement of the centre of vehicle for different camber angles with 0.3 rad fork angle and (b) Lateral displacement vs. longitudinal displacement of the centre of vehicle for different castor angles with 0.2 rad camber angle

3.7 CONCLUSIONS

Bond graph of bicycle vehicle model has been developed to see the effect of camber angle and fork angle on ABS while manoeuvrings a curved path. It has been concluded that camber angle decreases the stopping distance as well as turning radius of the vehicle. On the other hand, fork angle increases the turning radius of the vehicle. Increase in camber angle reduces the longitudinal speed of the vehicle while turning. But increase in fork angle increases the longitudinal

speed of the vehicle. For a fixed value of turning radius, if we increase the castor angle, camber angle will also increases.

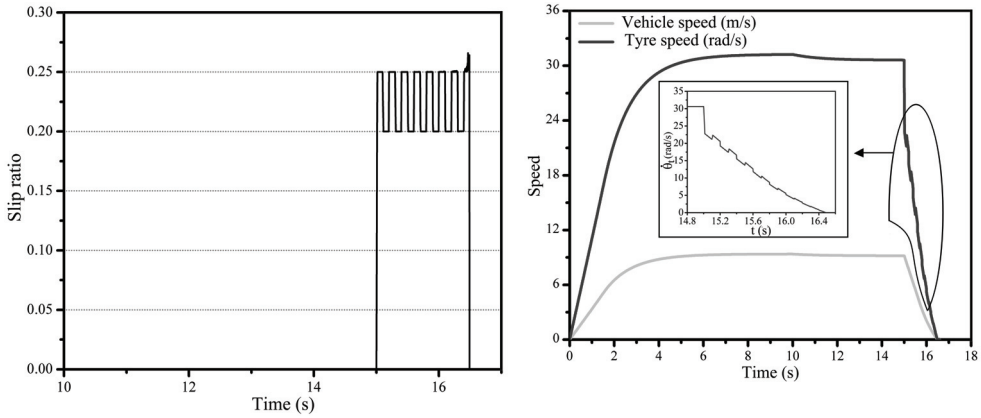

(a) (b)

Fig. 3.16 (a) Slip ratio with time and (b) vehicle speed and wheel speed with time

It is seen from the simulation results that for a particular value of castor angle and camber angle, the stability of the vehicle can be increased as well as the vehicle moves through the specified road. This model can be extended to the four wheel vehicle model with load transfer effect. In the next chapter, the variable camber angle mechanism can be developed along with ABS.

CHAPTER 4
VARIABLE CAMBER MECHANISM FOR QUARTER CAR VEHICLE MODEL

4.1 INTRODUCTION

Modern vehicles have many complex assemblies which adjust themselves according to vast range of dynamic conditions imposed by the road slope, road-surface, load shifts, pitch, turns, *etc.* To adapt to such conditions, most of the static systems are replaced with complex mechanisms to adapt the dynamic-environment encountered during driving. The parameters like camber and fork angles are generally locked to some pre-set values. These parameters must be varied in some acceptable ranges to efficiently handle different dynamic conditions.

It is desired to provide vehicle with variable wheel camber which varies in a range for better performance and vehicle stability. When the vehicle is steered, the dynamic variable camber mechanism adjusts the wheels camber in dynamic optimal proportion. Camber angle is the inward or outward tilt of the wheel with respect to the vehicle viewing from the top. When the top of the wheel is tilted towards the vehicle, it is said to have negative camber angle. If the top of the wheel is tilted away from the vehicle, it is said to have positive camber. During manoeuvring a curved path, the inward wheel must have positive camber and the outer wheel must have negative camber for larger contact with road surface. Thus leads to better vehicle performance in various road conditions.

A variable camber suspension system (VCSS) having sensor, controller and camber adjuster was developed by Choudhery [**45**]. A suspension system with camber adjustment mechanism while manoeuvring a curved path lowers and draws inward the upper A-arm of the outer front tyre, thus provides the negative camber angle to the wheel [**46**]. Two wheelers always have positive camber angle either they are manoeuvring left or right. Two wheelers require large camber angle and small steering angle while turning, whereas, four wheelers require large steering angle and small camber angle.

First, a variable camber mechanism is designed and then its bond graph is modelled for the dynamic analysis of a quarter car model. Unequal length A-arms suspension system is modified accordingly to get the dynamic variation in camber angle. Quarter car model is used in the simulation.

4.2 DEVELOPMENT OF VARIABLE CAMBER MECHANISM

Steering of the vehicle determines the position of the wheel on the ground and the stresses imposed on the wheels such that the wheel is in best position for the transmission of forces and moments. When the vehicle is manoeuvring a curved path, the centrifugal forces cause the vehicle body to roll, resulting in load transfer from the inner wheels to the outer wheels. This causes the compression of suspension of inner wheels and extension of suspension of outer wheels. The roll provides negative camber to the outer wheels in conventional unequal length A-arms suspension. For conventional unequal length A-arms suspension, when wheels are encountered with ride height changes, provides suboptimal wheel camber because the right wheel provides left steering effect and left wheel provides right steering effect. Thus, for conventional independent unequal length A-arms suspension, each wheel provides its own steering effect when vehicle travels on variable height path. This condition is called bump steer. This action causes decrease in direction stability and ride performance. So, it is desired to have zero camber changes while moving straight ahead and dynamic variation in wheel camber while manoeuvring.

The present variable camber mechanism provides zero changes in camber angle while moving straight ahead, thus removes bump steer and provides suitable camber while manoeuvring a curved path. This is done by providing a connection with dynamic variation in camber and vehicle steering system. The complete mechanism is discussed later.

Figure 4.1 shows the variable camber mechanism and steering system. The system includes left front wheel, lower A-arms connected to the vehicle frame, upper A-arms connected to the vehicle frame and camber adjustment mechanism, a steering rack driven by a steering gear. The upper A-arm is connected to the lower A-arm through hub carrier. The lower A-arms are connected to the frame through pivot joints. Thus, lower A-arm is allowed to

move up and down in an arc. The hub carrier is attached to the free end of the tie rod at a ball joint connection.

The upper A-arm is also connected to the slide mount through pivot joints. The slide mount is guided by a guide rod that freely penetrates through the guide rod slot of the slide mount. The guide rod is attached to the frame at upper attachment point and lower attachment point. Upper attachment point is not shown in Fig. 4.1. The slide mount has a guide plate roller.

The tie rod is connected through ball joint to the guide plate. The guide plate includes a guide groove. The roller of the slide mount fits in this groove. The guide plate is placed horizontally in the chassis and attached to the steering rack of the vehicle steering mechanism. The guide rod transfers the motion of steering rack to the tie rod and also guides the slide mount roller in the guide groove.

The flat portion of the groove ensures zero camber angle while moving straight ahead. The profile of the guide grove is such that it limits the maximum and minimum camber angle. Figure 4.1 shows the transition of the vehicle from straight operating condition to left turn. As the guide plate moves, the slide mount follower rolls within the guide plate groove. As the guide plate moves the left direction, the guide plate's grove forces the slide mount follower to move outward and is forced upward by the upward portion of the guide plate groove. The follower thus forces the slide mount to slide upward and outward, thus provides positive camber angle to the left wheel.

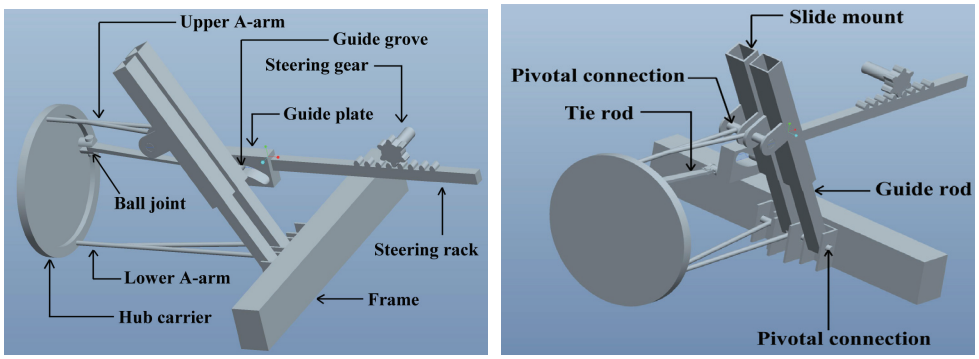

(a) (b)

Fig. 4.1 Different views of variable camber mechanism

4.3 BOND GRAPH MODEL OF VARAIBLE CAMBER MECHANISM

The working of Variable Camber Mechanism (VCM) is analysed for its modelling. Since, the variable camber mechanism is attached with steering mechanism. Therefore, while taking left turn, steering wheel is rotated counter clockwise direction looking from top, the steering gear also rotates in the same sense and the rack is pushed inwards for the left wheel.

4.3.1 Kinematic analysis of variable camber mechanism

For the development of the bond graph of variable camber mechanism, its basic fundamental equations should be formulated first on which the bond graph is to be portrayed. The moment acting on the steering gear is in x-direction. Therefore $(\dot{\theta}_x)$ is the input to the steering gear. Due to this, the follower in the groove moves in y-z plane. The movement is shown in Fig. 4.2(a). The equations of motions derived from simple kinematic relation are given by

$$\dot{y}_1 = \dot{y} - \dot{\theta}_x a Sin\theta \tag{4.1}$$

$$\dot{z}_1 = \dot{z} + \dot{\theta}_x a Cos\theta \tag{4.2}$$

Where, $(\dot{y}_1, \dot{z}_1)$ are the velocities at the ball joint of tie rod at the wheel end and $(\dot{y}\ , \dot{z}\ )$ are the velocities at the centre of the follower. *a* is the distance between them.

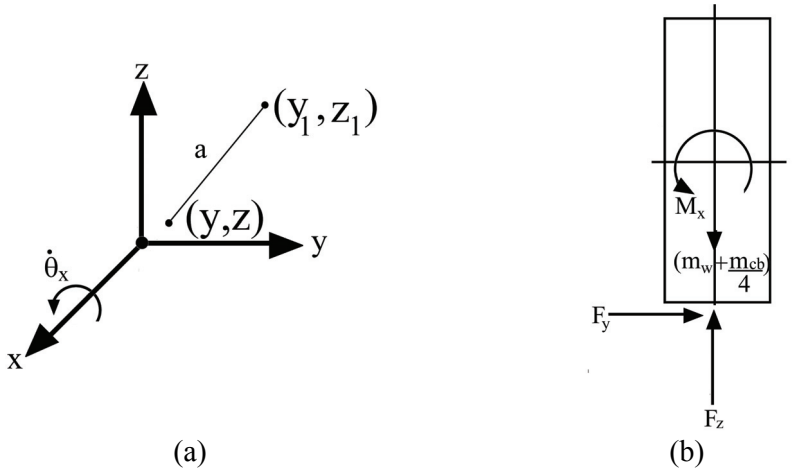

Fig. 4.2 (a) Displacement of the wheel due to rotation of steering gear and (b) diagram of quarter car model

Bond graph is constructed on the basis of these above equations. The wheel displacements in different directions are measured to check whether it follows the desired profile. For this, planar wheel (in the y-z plane) quarter car model is considered here for the analysis. y-z plane is taken for the analysis of the wheel. The quarter car model is discussed later.

4.3.2 Bond graph model

Bond graph model of the variable camber mechanism is shown in Fig. 4.3. The torque applied by the driver of the vehicle is denoted by SE element connected at the 1-junction. The inertia of the driving wheel is presented by I-element connected at the same 1-junction. The steering gear is expressed by TF-element with gear ratio μ. The velocity of the guide plate in the y-direction and the rotational speed of the pinion about x-axis, modulate the cam profile. The velocities of the centre of the follower in y and z-direction and rotational speed about x-axis are represented by three numbers of 1-junctions. Equations (4.1–4.2) are used to calculate the velocity at the ball joint of the tie rod. The complete profile has two parts—one for positive camber and the other for negative camber. The cam may be represented as source of flow (SF). The linear and rotational stiffness of the bar element is represented by C-element connected at the 0-junction. So, input to the wheels are forces F_y and F_z and moment M_x.

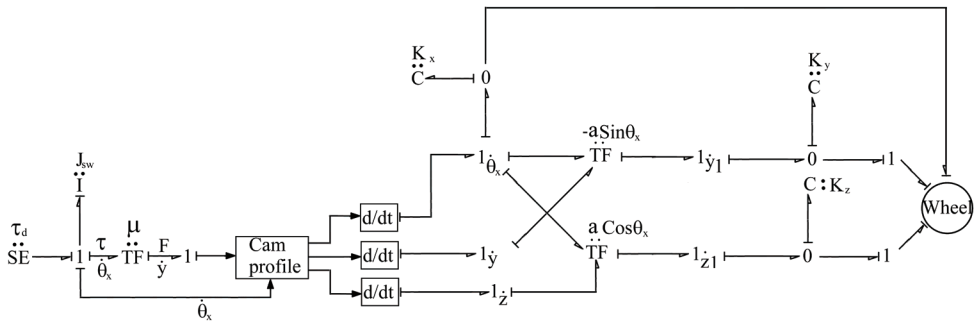

Fig. 4.3 Bond graph model of variable camber mechanism

4.3.3 Quarter car model

The schema of quarter car model is shown in Fig. 4.2 (b). The quarter car model is used here to implement the variable camber mechanism. The wheel is in the y-z plane. As shown in the Fig. 4.2(b), F_z is the force in the vertical direction of

the vehicle. Similarly, F_y is the force acting in the lateral direction of the wheel. Here, m_w is mass of the wheel and m_{cb} is the mass of the vehicle. The equations of motion of vehicle is given by :

$$\left(m_w + \frac{m_{cb}}{4}\right)\ddot{y} + F_y = F_{ym} + \left(m_w + \frac{m_{cb}}{4}\right)g\sin\alpha_E + m_w\dot{\alpha}_E\dot{Z} - R\dot{y} - \left(K_v Z_t + R_v \dot{Z}_t\right)\sin\alpha_E \quad (4.3)$$

$$I_x\ddot{\alpha}_E = F_y R_w - R\dot{\alpha}_E + F_{\alpha m} \quad (4.4)$$

Where F_y, F_{ym} and $F_{\alpha m}$ are the force acting on the wheel calculated from Pacejka's magic formula, force acting on the wheel in y -direction and torque acting on the wheel due to camber mechanism respectively.

4.3.4 Bond graph of Quarter car model

The bond graph of quarter car model is shown in Fig. 4.4. The wheel is modelled as rigid body with three degrees of freedom. The tyre-road normal contact force and the gravity force acts along Z-axis. The three effort inputs are given to $1_{\dot{y}}$, $1_{\dot{z}}$ and $1_{\dot{\alpha}}$ junction. The stiffness and damping of the tyre is represented by C and R respectively. The brake torque is applied to the wheel at 1 junction of the wheel.

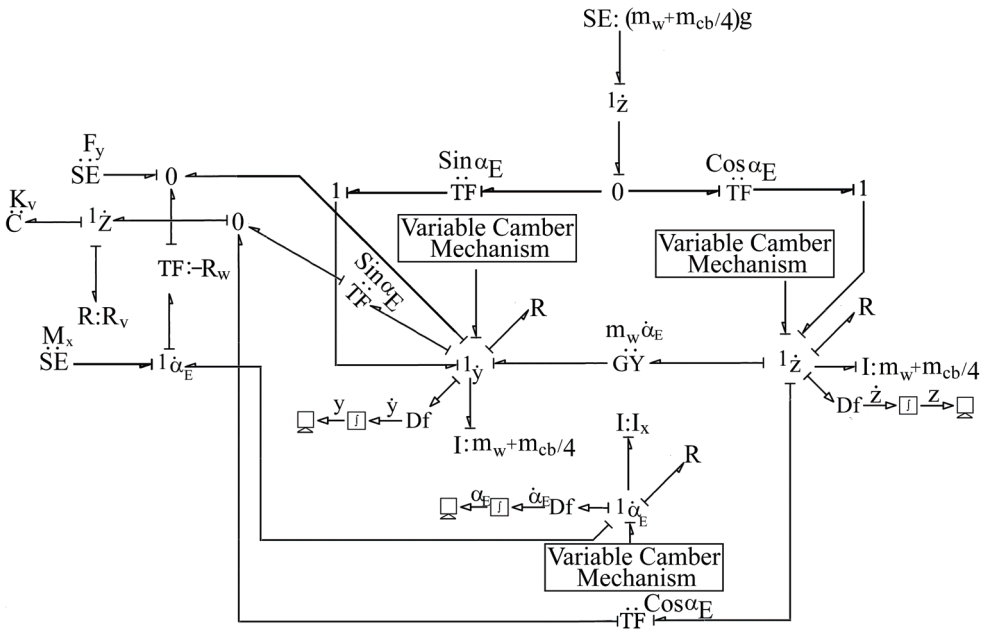

Fig. 4.4 Bond graph model of quarter car model

4.4 PARAMETER VALUES AND SIMULATION RESULTS

The analysis of variable camber mechanism is done by using quarter car model. The complete parameter values used in the simulation are given in Table 4.1. Pacejka's magic formula (refer Eq. 3.6) is used for the calculation of the lateral force.

Table 4.1: Parameter values of variable camber mechanism

Subsystem	Parameter values			
Wheel	m_w =15 Kg	R_w =0.3 m	I_x =20 Kg m^2	K_w =300000 N/m
	R_w =200 N s/m	R_y =10^8 N s/m	R_z =10^7 N s/m	R_α =0.0 Nm s/rad
Brake	D =117	C =1.2	E = –2	B =8.33

As the vehicle is manoeuvring a left turn, it is moving in the negative y direction and positive z direction. The profile of the guide grove is shown in Fig. 4.5. Angular rotation of 0.05 rad is given in x-direction. From the input data, the angle varies from 0–0.05 rad, displacement input in y-direction varies from 0 to (–52.35) and displacement input in z-direction varies from 0 to 13.19 for left turn.

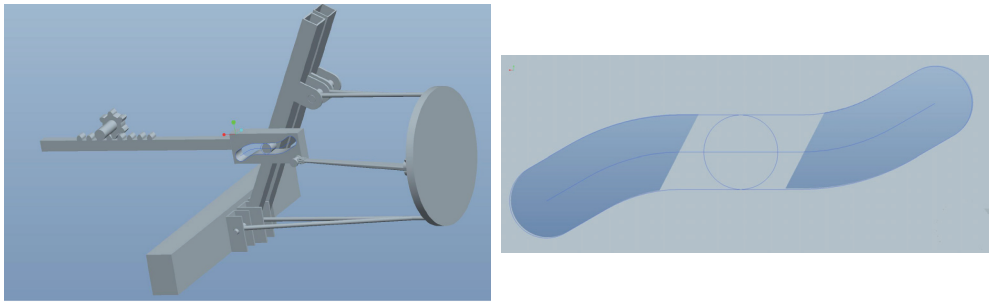

(a) (b)

Fig. 4.5 The profile of the guide of variable camber mechanism

Fig. 4.6(a) shows the displacement in y-direction. Clearly the displacement is from 0 to (–52.35) which clarify that the wheel is displaced exactly according to the input in y-direction. Similarly, the displacement in the z-direction is shown in Fig. 4.6(b). It also shows that wheel is moved by the

exact distance as the input data. Figure 4.7(a) is the angular displacement in x-direction. Since, the input of 0.05 rad is given, it is quite clear that the wheel is displaced by the same amount. Figure 4.7(b) shows the similar curve is generated by the model. Hence, positive camber angle is achieved by the left wheel of the vehicle while taking a left turn.

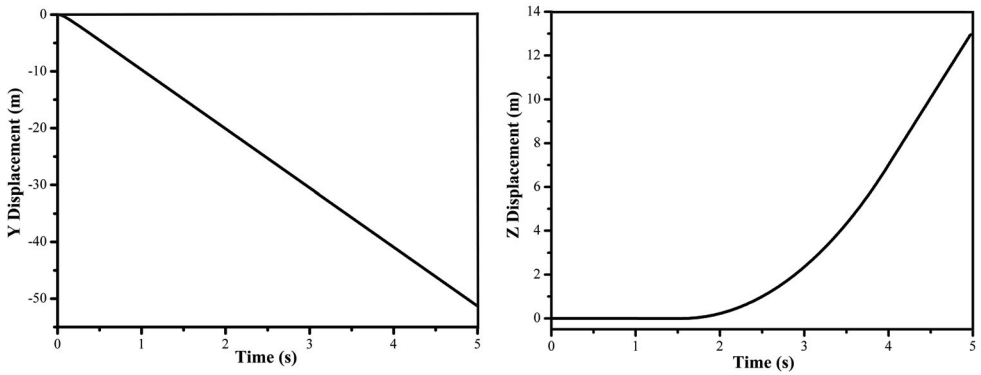

(a) (b)

Fig. 4.6 (a) The lateral displacement of the wheel and (b) vertical displacement of the wheel

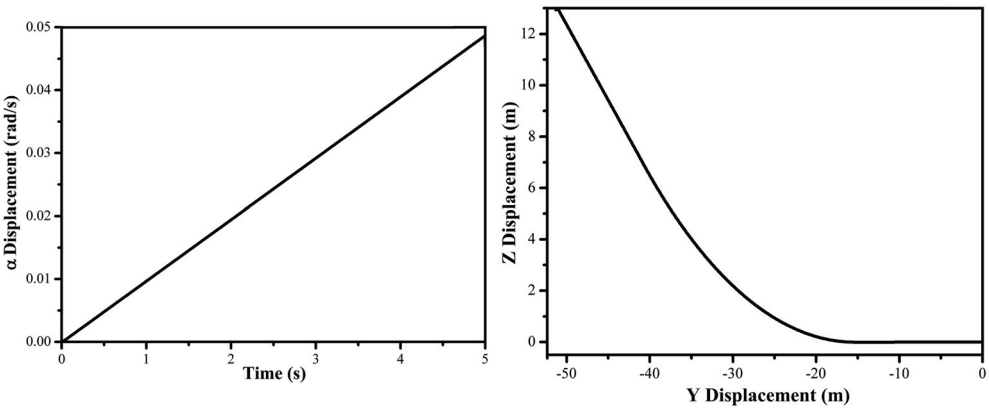

(a) (b)

Fig. 4.7 (a) Angular displacement of the wheel is x direction and (b) the graph between lateral and vertical displacement

4.5 CONCLUSION

The variable camber mechanism attached with steering system is developed and this provides accurate camber angle to the wheels while turning. The bump steering is completely eliminated while moving on road with variable height. The

straight portion of the guide grove ensures that no camber angle is attained while moving straight. The wheel attains the required camber angle while cornering. Thus improves the vehicle stability and ride quality.

CHAPTER 5

VARIABLE CAMBER MECHANISM FOR FOUR WHEEL VEHICLE MODEL

5.1 INTRODUCTION

The use of automobile is increasing worldwide which has motivated in the development of number of driver assisted safety features. Modern automobile vehicles are increasingly dependent on electromechanical sub-systems which include sensors, actuators and feedback control systems and assist vehicle stability, improves ride quality, reduce traffic congestions, increase fuel economy and reduce vehicle emissions. Continuous improvement is required in the existing control systems for more and more improvement in the vehicle performance.

Antilock braking system is a very important safety feature in modern four wheel vehicle. Its uses an on-off control strategy to prevent the wheels from locking even in situations where very hard brakes are applied and thus prevents the wheels from skidding and helps in better steering of the vehicle. Now-a-days, more and more stress is laid on improvement in the conventional ABS system. Numbers of factors are considered in the ABS algorithm which includes slip control, friction coefficient between tyre and road, wheel deceleration, longitudinal braking force and many more. The sudden jumps in the road tyre friction coefficient due to change in the road conditions also changes the amount of steering required while maneuvering a curved path and does not follow the nominal path . For roads with slippery surface, the vehicle travels on a trajectory with larger radius and this condition is called under steering. Similarly, for roads with higher friction coefficient, the vehicle follows a trajectory with small radius and this condition is called over steering. Differential-braking based system can be used to avoid such situation. By increasing the brake pressure on the left wheels as compared to the right wheels, a counter-clockwise yaw moment is generated and by increasing the brake pressure on the right wheels as compared to left wheels, clockwise yaw moment is generated.

There is also load transfer from the rear axle to the front axle during braking and vise versa during acceleration. The load transfer is from inner wheels

to outer wheels while maneuvering a curved path. For accurate prediction of ABS system performance, proper accounting of load transfer is to be required. The load transfer mechanism during braking and turning cannot be represented in the quarter car or bicycle model. Therefore, a four wheel model should be used for accurate prediction of system performance.

For reducing stopping distance and steering angle, camber angle is to be introduced in the four wheel model. Camber angle is represented as the angular moment applied to the tyre about x-axis of the vehicle. Camber angle is said to be positive, when the top of the tyre is tilted outwards with respect to the body of the vehicle and is negative when the top of the tyre is tilted inwards. Variable camber mechanism is already discussed in Chapter 4. Therefore, camber angle adds one more rotation input to the tyre along with steering input and braking torque.

Bond graph modelling is a pictorial representation of physical systems. It is vastly used for the analysis of system lies in different energy domains. It is best used in the modelling and formulation of system equations lies in different energy domains. It is not a numerical solution tool. Bond graphs gives the equation of motion with static and dynamic constrains but does not give the numerical solution directly. One has to use some numerical technique to get the solution.

5.2 MODELLING OF FOUR WHEEL VEHICLE

The four wheel vehicle system comprises of seven subsystems. These are vehicle body, suspension, wheel, steering, variable camber mechanism, (antilock) braking system and differential. To assist the vehicle steering and for short stopping distance, variable camber mechanism may be used. Therefore, modelling of each subsystem is done to represent the complete model. The word bond graph of the full vehicle model is shown in Fig. 5.1 where the bonds represented by double lines are multiple bonds.

The conversion of flow variables from body fixed frame to inertial frame and vice versa is done through coordinate transformation (CTF) block. The flow variables at the interface of different subsystems are shown in Fig. 5.1. The complementary power variables are omitted to maintain the clarity. The steering wheel, antilock braking system and the variable camber mechanism (VCM) are

represented by scalar bonds to the axle. Similarly, the electrical dc motors are connected to the rear wheels and the vehicle body by scalar bonds. The wheels are connected with the vehicle body through suspension.

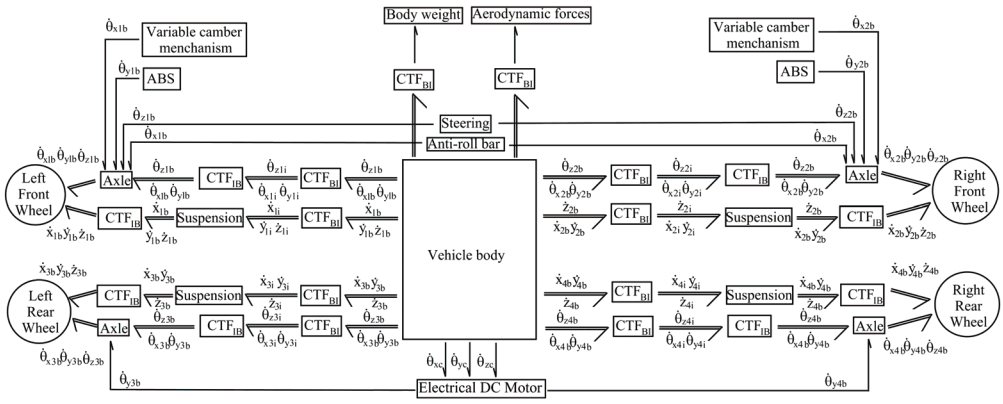

Fig. 5.1 Word bond graph of four wheel vehicle model

5.2.1 Bond graph of vehicle body

The bond graph modelling of the vehicle body is presented in this sub-section. The vehicle is assumed to be symmetric with respect to the longitudinal axis. Three linear displacements along the three body-fixed axes and three rotation motions about those axes are used to describe the vehicle body. So it is a 6-DOF rigid body. The rotary motion of the body is defined by the Cardan angles. The Newton-Euler equations with attached body fixed axes aligned with principle axes of inertia are used for the modelling the vehicle body. The Newton-Euler equations of the vehicle body with attached body fixed axes aligned with principal axes of inertia are given by

$$\sum F_{\mathrm{x}} = m_{\mathrm{c}}\ddot{x}_{\mathrm{c}} + m_{\mathrm{c}}(\dot{z}_{\mathrm{c}}\dot{\theta}_{\mathrm{cy}} - \dot{y}_{\mathrm{c}}\dot{\theta}_{\mathrm{cz}}) \tag{5.1}$$

$$\sum F_{\mathrm{y}} = m_{\mathrm{c}}\ddot{y}_{\mathrm{c}} + m_{\mathrm{c}}(\dot{x}_{\mathrm{c}}\dot{\theta}_{\mathrm{cz}} - \dot{z}_{\mathrm{c}}\dot{\theta}_{\mathrm{cx}}) \tag{5.2}$$

$$\sum F_{\mathrm{z}} = m_{\mathrm{c}}\ddot{z}_{\mathrm{c}} + m_{\mathrm{c}}(\dot{y}_{\mathrm{c}}\dot{\theta}_{\mathrm{cx}} - \dot{x}_{\mathrm{c}}\dot{\theta}_{\mathrm{cy}}) \tag{5.3}$$

$$\sum M_{\mathrm{x}} = J_{\mathrm{cx}}\ddot{\theta}_{\mathrm{cx}} - \dot{\theta}_{\mathrm{cy}}\dot{\theta}_{\mathrm{cz}}(J_{\mathrm{cy}} - J_{\mathrm{cz}}) \tag{5.4}$$

$$\sum M_{\mathrm{y}} = J_{\mathrm{cy}}\ddot{\theta}_{\mathrm{cy}} - \dot{\theta}_{\mathrm{cz}}\dot{\theta}_{\mathrm{cx}}(J_{\mathrm{cz}} - J_{\mathrm{cx}}) \tag{5.5}$$

$$\sum M_{\mathrm{z}} = J_{\mathrm{cz}}\ddot{\theta}_{\mathrm{cz}} - \dot{\theta}_{\mathrm{cx}}\dot{\theta}_{\mathrm{cy}}(J_{\mathrm{cx}} - J_{\mathrm{cy}}) \tag{5.6}$$

The vehicle body is modelled as a rigid body and has six degrees of freedom, *i.e.,* pitch, roll, yaw, heave, surge and sway motions. The rigid body motion of the vehicle body is described with respect to a coordinate system rotating and translating with it. This local coordinate frame attached at the centre of mass of the body is assumed to be aligned with the inertial principle axes. First three equations (Eq. (5.1)–(5.3)) are Newton's equations which represents pseudo-forces appear due to the use of body-fixed or non-inertial frame. Last three equations (Eq. (5.4)–(5.6)) are Euler's equations which accounts for the gyroscopic moment. The liner and angular velocities used in the above Newton-Euler equations are velocities as seen from a frame that is momentarily aligned with the body-fixed principle axes.

Euler's equations can be represented in the bond graph form through Euler junction structure (EJS). To draw EJS let us consider a rigid body of mass (m), moment of inertia about principle axes $(\mathrm{x},\mathrm{y}\ and\ \mathrm{z})$, as $(I_{xx}, I_{yy}\ and\ I_{zz})$, angular velocities momentarily aligned along body fixed principle axes $(\omega_x, \omega_y\ and\ \omega_z)$, as external moment component as $(M_x, M_y\ and\ M_z)$, and external forces components as $(F_x, F_y\ and\ F_z)$. The EJS for a rigid body is shown in Fig. 5.2(a). Similarly, Newton's equations are modelled by using gyrator ring structure.

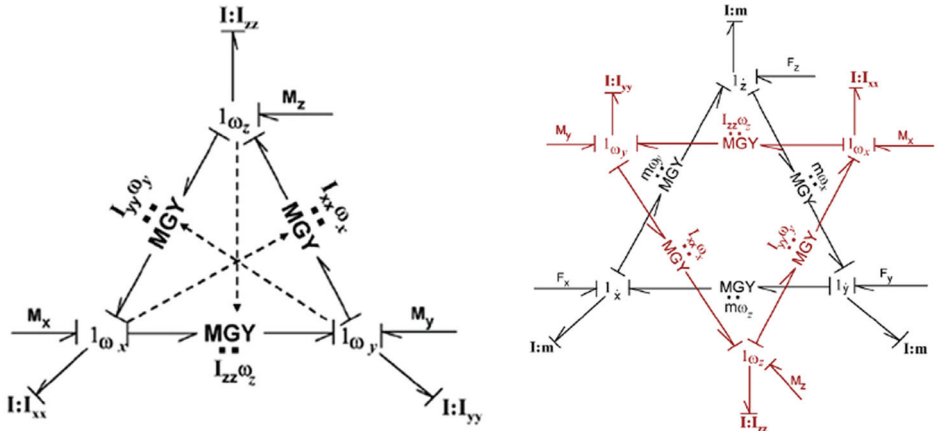

Fig. 5.2 Bond graph model of (a) Euler equation and (b) Newton-Euler equation [20].

The Newton-Euler's equations are represented in bond graph form by combining both junction structures to form star shaped junction structure as shown in Fig. 5.2(b). So, Fig. 5.2(b) is the main building block of bond graph modelling of vehicle body. The coordinate transformation block (CTF) are used in several places to convert flow variables from body fixed frame to inertial frame and from inertial frame to body fixed frame using rotation matrix.

For the vehicle body, $\omega_{\mathrm{x}} = \dot{\theta}_{\mathrm{cx}}$, $\omega_{\mathrm{y}} = \dot{\theta}_{\mathrm{cy}}$, $\omega_{z} = \dot{\theta}_{cz}$, $I_{\mathrm{x}} = J_{\mathrm{cx}}$, $I_{\mathrm{y}} = J_{\mathrm{cy}}$ and $I_{\mathrm{z}} = J_{\mathrm{cz}}$. The suspension reference point coordinates are $x_{\mathrm{i}} = a$, $y_{\mathrm{i}} = c$, and $z_{\mathrm{i}} = -h$. The bond graph model of the vehicle body is shown in Fig. 5.3. It models the vehicle body inertia and transforms the three liner and three angular velocities into velocities at reference suspension points of all the four wheels. The inertia is coupled by a pair of gyrator rings. Three set of forces and moments act on the vehicle body. First, vehicle body weight and aerodynamic forces (R_{aero}) in the inertial frame act on the body in non-inertial frame through coordinate transformation (CTF). Secondly, engine torque which is in wheel frame is first transformed from wheel to body fixed frame and then from body fixed to vehicle body fixed frame to act on the body. Thirdly, the suspension forces and moments which act in the inertial frame are transformed to get forces in body fixed frame.

5.2.2 Bond graph model of wheels

The bond graph model of wheel is similar to that of vehicle body. The wheel is modelled as rigid body with six degrees of freedom. The inertias are coupled by a pair of gyrator rings as shown in Fig. 5.4.

There are some basic differences between the vehicle body model and the tyre model. The suspension reference points in the vehicle body are fixed points whereas, the tyre-road contact point in the wheel is not a point fixed on the wheel. It changes as the wheel rotates about the axle. The second difference is that the wheel rotation about its axle axis does not change its orientation in the inertia frame. Here, the wheel and its axle are assumed to be rotationally symmetric about an axis.

The tyre-road normal contact forces and the gravity forces $(\mathrm{SE}: m_{\mathrm{w}} g)$ acts along z-axis. The vertical velocity of the wheel is calculated through a set of

transformation at a 0 junction where the vertical stiffness and damping of the tyre (K_t and R_t elements) are modelled. The angle ϕ used in the transformation is the wheel tilt with respect to the ground, *i.e.*, the angle of rotation of the wheel about X-axis. The tilt angle may include additional camber angle.

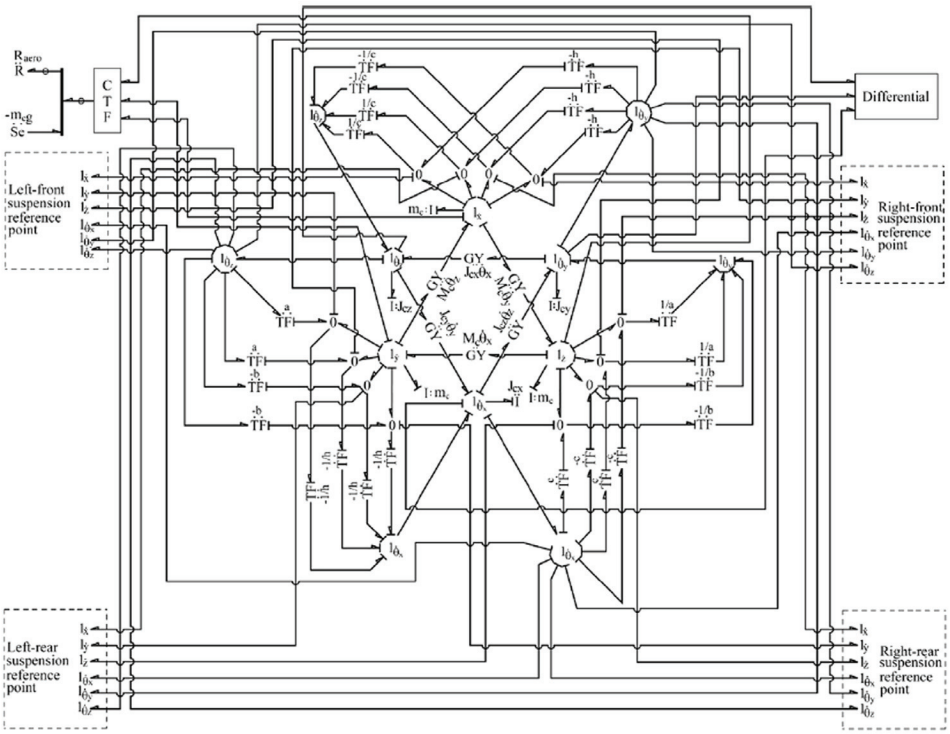

Fig. 5.3 Bond graph model of vehicle body [20].

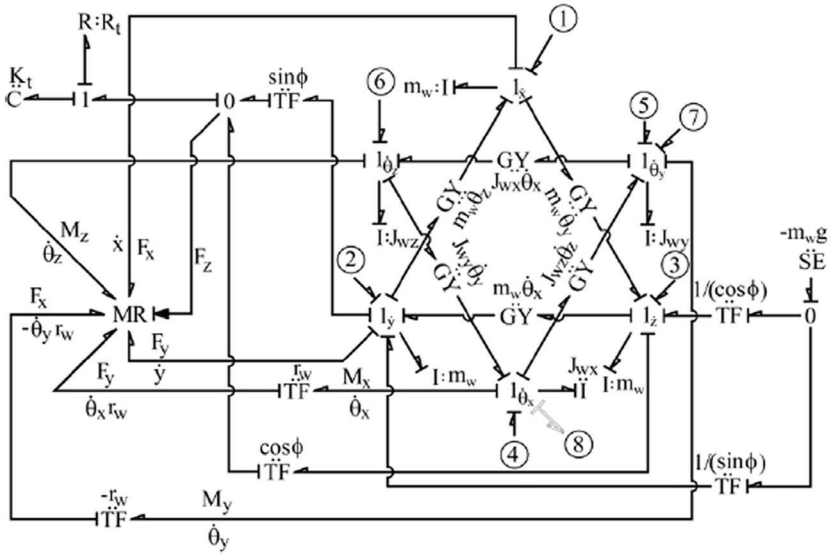

Fig. 5.4 Bond graph model of wheel [20].

Port 1–6 are connected to the corresponding velocities of the suspension reference points. The brake torque is applied to the front wheel at port 7 and engine torque is supplied to the rear wheel through the port7. The steering torque is applied through port 4.

5.2.3 Bond graph model of steering system

The Ackermann's formulae are the basic building block of bond graph model of steering system. The schema is shown in Fig. 5.5(a). The Ackermann's equations are given by

$$m_1 = \left[\frac{(a+b)\cos^2\delta_1 + c\tan\delta_1\cos^2\delta_1}{(a+b)\cos^2\delta - c\tan\delta\cos^2\delta} \right] \tag{5.7}$$

$$m_r = \left[\frac{(a+b)\cos^2\delta_2 - c\tan\delta_2\cos^2\delta_2}{(a+b)\cos^2\delta + c\tan\delta\cos^2\delta} \right] \tag{5.8}$$

The bond graph of steering system is shown in Fig. 5.5(b). The rotational velocity $(\dot{\theta}_{\text{ref}})$ applied to the steering wheel is represented as SF which is connected to the 1 junction. The rate of rotation of the left wheel and right wheel about the z axis are represented at $1_{\delta 1}$ and $1_{\delta 2}$ junctions. The modulus of the transformers are taken from Eq. (5.7–5.8).

5.2.4 Bond graph of variable camber mechanism

The schema of wheel camber representation is shown in Fig. 5.6. It is concluded from the sketch that

$$\left.\begin{aligned} \tan\delta &= \frac{h_1 + h_2}{x + c} \\ \tan\delta_1 &= \frac{h_1 + h_2}{x + 2c} \\ \tan\delta_2 &= \frac{h_1 + h_2}{x} \end{aligned}\right\} \tag{5.9}$$

Therefore, while taking left turn the left wheel should have less camber angle and right wheel should have more camber angle. It is calculated that, for $\delta = 0.1\,\text{rad}$, the camber angle for the left wheel is 0.087 rad and for the right is 0.116 rad.

The bond graph is shown in Fig. 5.6(b). The angular velocity $\left(\dot{\theta}_{\text{ref}}\right)$is applied to the 1 junction. The rate of rotation of the left wheel and right wheel about the x axis are represented by $1_{\alpha 1}$ and $1_{\alpha 2}$ junctions. The moduli of the transformers are calculated from equations given by

$$m_{\text{l}} = \left[\frac{(h_1 + h_2)\cos^2 \alpha_1 + c \tan \alpha_1 \cos^2 \alpha_1}{(h_1 + h_2)\cos^2 \alpha - c \tan \alpha \cos^2 \alpha} \right] \tag{5.10}$$

$$m_{\text{r}} = \left[\frac{(h_1 + h_2)\cos^2 \alpha_2 - c \tan \alpha_2 \cos^2 \alpha_2}{(h_1 + h_2)\cos^2 \alpha + c \tan \alpha \cos^2 \alpha} \right] \tag{5.11}$$

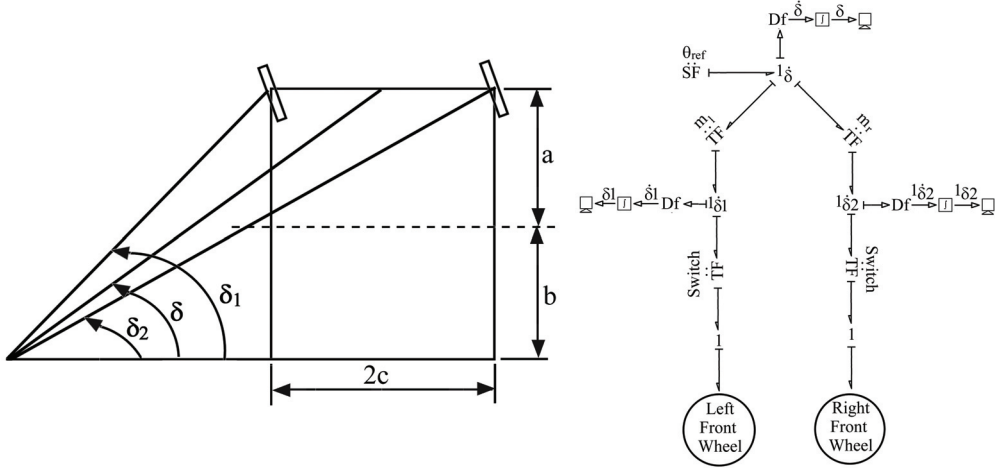

(a) (b)

Fig. 5.5(a) Schema of steering system and (b) its bond graph.

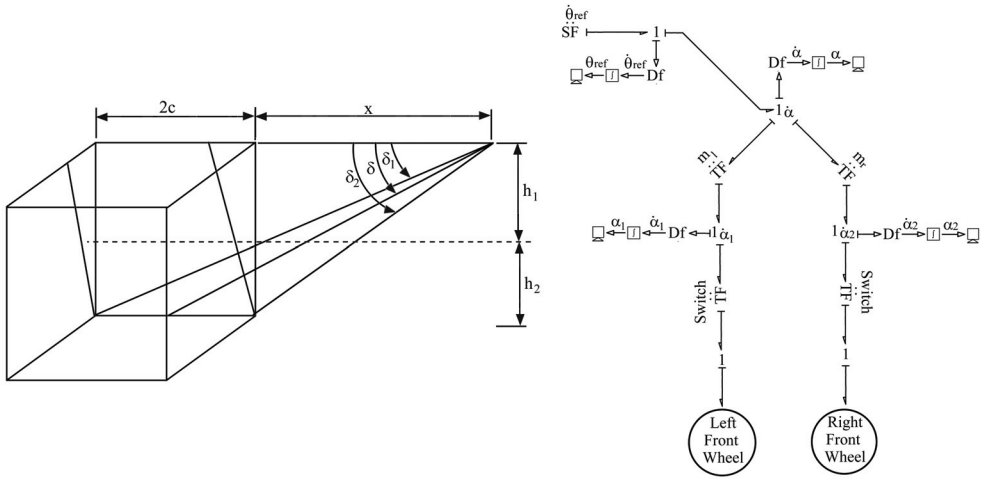

(a) (b)

Fig. 5.6 (a) Schema of wheel camber and (b) its bond graph.

5.3 PARAMETER VALUES AND SIMULATION RESULTS

The vehicle behaviour is obtained from the vehicle dynamic model by giving reasonable input to various parameters. The parameter values used in the simulation is given in Table 5.1.

Table 5.1: Parameter values of 4-wheel vehicle model with camber mechanism

Subsystem	Parameter values			
Vehicle body	m_c =1600 Kg	J_{cx} =260 Kgm^2	J_{cy} =1110Kgm^2	J_{cz} =1370Kgm^2
	a =0.9 m	b =1.5 m	c =0.7 m	
Suspension	K_{sx} =10^7 N/m	R_{sx} =2000 Ns/m	K_{sy} =10^7 N/m	R_{sy} =2000Ns/m
	K_{sz} =80 kN/m	R_{sz} =500 N s/m	K_{stx} =10^{7}Nm/rad	R_{stx} =2000Nms/rad
	K_{sty} =0	R_{sty} =0 N ms/rad	K_{stz} =10^{6}Nm/rad	R_{stz} =360Nms/rad
Wheel	m_w =15 Kg	J_{wx} =0.1Kg m^2	J_{wy} =0.2 Kg m^2	J_{wz} =0.1 Kg m^2
	r_w =0.3 m			
Brake	σ_{low} =0.2	σ_{high} =0.25	s_g =0.01	k_g =250 N/m
	r_{bd} =0.15m	R_{lm} =0.04 N s/m	K_{ca} =10^4 N/m	K_{re} =10^6 N/m
	l_a =1 m	C_1 =1.029	C_2 =17.16	C_3 =0.523
	C_4 =0.03			
Steering wheel	J_{sw} =1 Kg m^2	δ =0.24 rad		
Camber mechanism	h_1 =0.25	h_2 =0.25	α =0.1 rad	

5.3.1 Effect of camber angle

Initially, the vehicle starts from rest and it attains a speed of 9.24 m/s at 3.8s. Camber angle of 0.1 rad is applied after 4s. As the wheel takes left turn, left wheel attains camber angle less than 0.1 rad and right wheel attains camber angle more than 0.1 rad. When camber angle is given to the wheel, there is some liner displacement in Y-direction and angular displacement in γ-direction as shown in Fig. 5.8. This shows that camber angle provides some additional steering effect. So, less steering is required with the presence of camber angle. When camber

angle is returned to zero on application, the vehicle continues to move in that direction but its path becomes straight and no longer remains a curve as shown in Fig. 5.9(b). So, camber angle guides the vehicle motion in the same sense as steering mechanism does. Hence, camber angle provides additional steering while maneuvering a curved path.

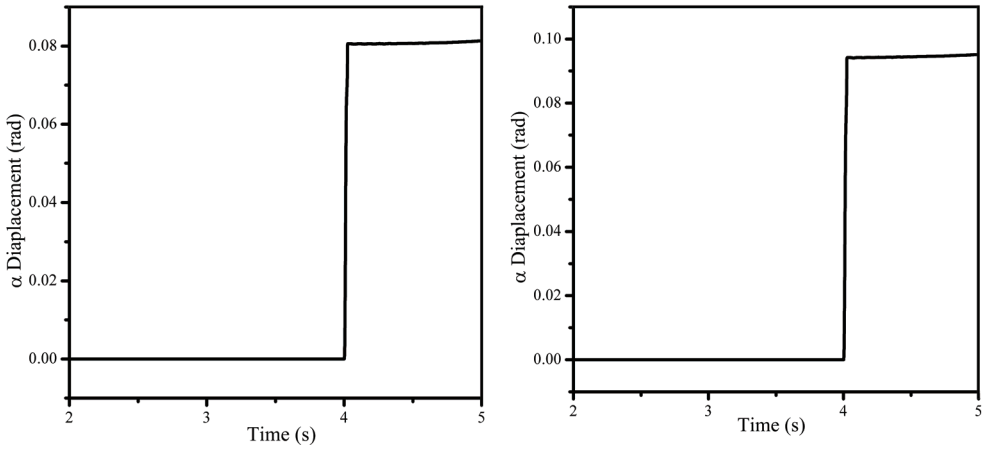

(a) (b)

Fig. 5.7 Application of camber angle for (a) left front wheel and (b) right front wheel.

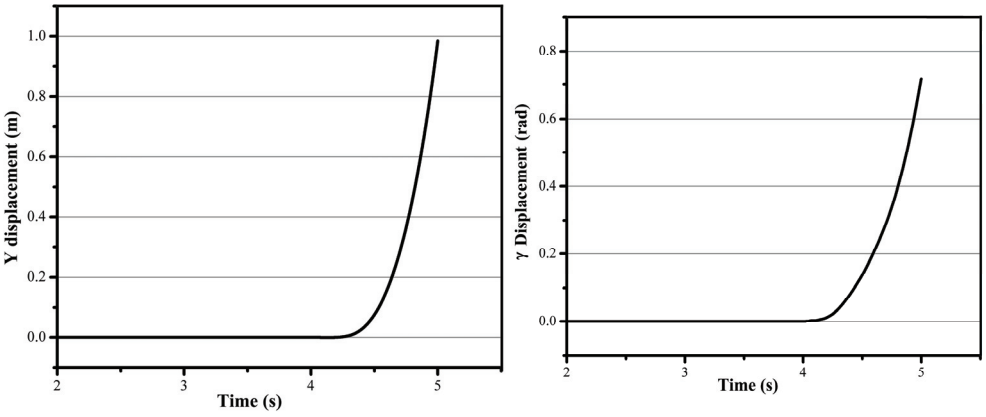

(a) (b)

Fig. 5.8 Displacement due to camber angle in (a) Y-direction of inertial frame and (b) γ-direction of body fixed frame.

A constant steering angle of 0.24 rad is applied at 4s to see the behaviour of the vehicle under constant steering angle. By giving a constant steering angle the vehicle is expected to move in a circular path with almost constant speed. Figure 5.10 shows the similar behaviour at constant longitudinal speed $(\dot{x})$ of 3.035 m/s and Fig. 5.10(b) sufficiently proves that the vehicle maneuvers in a curved path with constant radius.

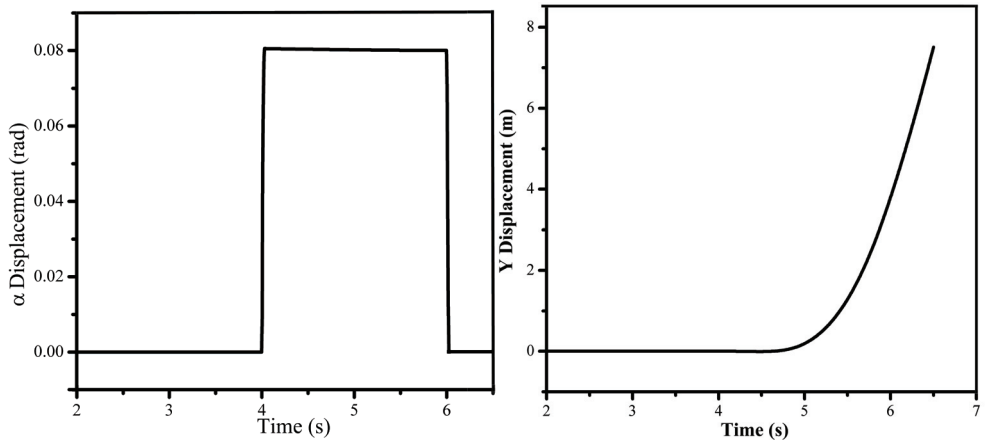

Fig. 5.9 (a) Application of camber angle with return and (b) displacement in Y-direction of inertial frame.

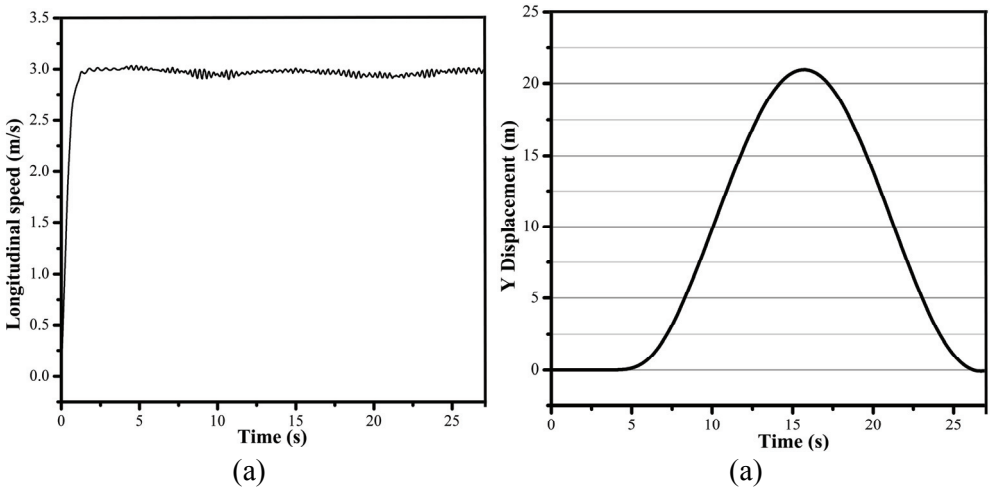

Fig. 5.10 (a) Longitudinal speed and (b) displacement in Y-direction for constant steering angle.

5.3.2 Antilock braking system

Antilock braking system is an on-off control strategy to prevent the wheels of the vehicle from locking. Different control parameters are considered in the ABS algorithm to prevent wheel lockage. Here, slip ratio is maintained by the ABS controller within two threshold values *i.e.*, 0.2–0.25. Figure 5.11 shows the behaviour of the vehicle under the application of antilock braking system. ABS is applied at 5s after starting. Figure 5.11(a) shows that the brake torque is applied in such a way so that vehicle slip is maintained between two threshold values. The ABS algorithm removes the brake pressure when slip exceeds the upper

threshold value and reapplies the brake pressure again when lower threshold is reached. Thus, vehicle stops with discrete deceleration and it does not stop continuously as shown by the wheel speed in Fig. 5.11(b). The vehicle stops smoothly without any wheel lockage.

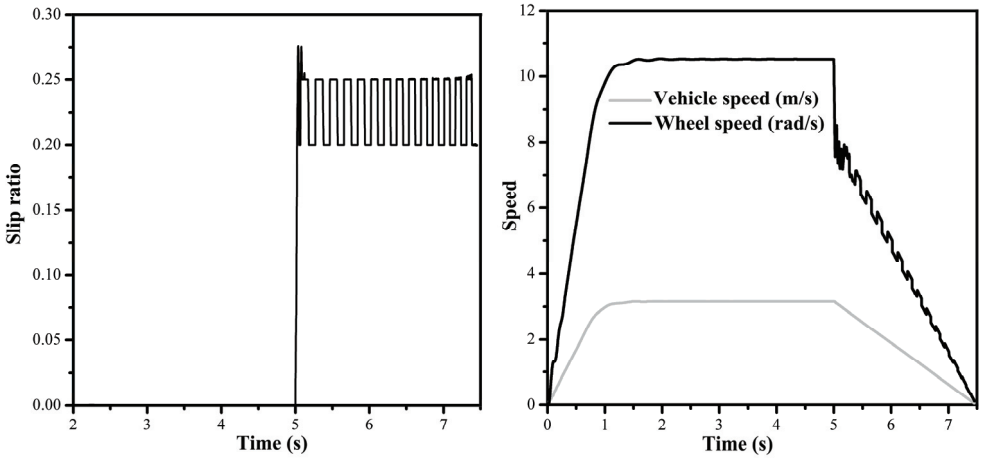

(a) (b)

Fig. 5.11 (a) slip ratio variation and (b) speed of vehicle and angular speed of wheel when brakes are applied.

5.4 CONCLUSION

In modern automobile world, the main motto is to provide such a technology which provides better handling on any road condition. It detects and assists the driver from any sudden change in road condition. Here, antilock braking system is developed which works on such a logic that it always maintain the slip ratio between 0.2–0.25 with respect to different road conditions. The effect of load transfer on braking and during maneuvering is also considered. Camber angle also assists the driver by providing additional steering while maneuvering a curved path. So, better steerability is achieved with the application of camber angle.

CHAPTER 6
CONCLUSIONS

6.1 CONCLUSION

Bond graph modelling of vehicles, variable camber mechanism and other mechanisms is done to study the effect of camber angle and fork angle. From the present work, it is concluded that turning radius as well as longitudinal speed decreases on increasing the camber angle up to certain limit without ABS and for no fork angle while turning. The turning radius increases while the longitudinal velocity decreases on increasing the fork angle without ABS and for no camber angle. It is concluded that for fixed turning radius, camber angle is proportional to fork angle. The increase in camber angle, decreases both stopping distance and turning radius while vehicle turns with ABS and for no fork angle. Whereas, stopping distance decreases but turning radius increases for the increase of fork angle with ABS and for no camber angle. For a fixed value of camber angle (0.2 rad) and fork angle (0.3 rad), both the stability of the vehicle is enhanced and vehicle follows the road on application of ABS. The slip ratio is maintained between 0.2–0.25 to obtain maximum frictional force between road-tyre interface.

Variable camber mechanism is developed in Chapter 4 which ensures zero camber angle while moving in a straight road when vehicle travels on variable height path. Cambering of the wheel is done while taking a turn with this mechanism. Some steering effect is also shown due to camber angle in Chapter 4. Less steering is required with the presence of camber angle. In Chapter 5, four wheel vehicle model was developed. The different components of the vehicle were modelled with the help of bond graph. The camber mechanism was developed on the basis of Ackermann steering mechanism in vertical plane. Formation of sine wave in longitudinal direction and almost constant longitudinal speed indicates that the vehicle is moving in a circular path for fixed steering angle. Formation of square wave for wheel speed represents the on-off strategy of antilock braking system.

6.2 FUTURE SCOPE OF WORK

Based on the thesis, the following areas of work are suggested for future exploration

- The range of variation of camber angle for which the vehicle have least turning radius and stopping distance.
- The range of variation of fork angle for which the vehicle have least turning radius and high speed stability.
- Refinement in the variable camber mechanism with the use of some logic controllers and sensors.
- Reduction in stopping distance without skidding of the wheel by developing more accurate control logic.

REFERENCES

[1] D. C. Karnopp, D. L. Margolis, R. C. Rosenberg, System Dynamics, Modelling and Simulation of Mechatronic Systems, John Wiley & Sons, NY, 2000.

[2] A. Mukherjee, R. Karmakar, A. K. Samantaray, Bond Graph in Modelling, Simulation and fault Identification, CRC Press, FL, 2006.

[3] D. Hrovat, J. Asgari, M. Fodor, Automotive Mechatronic Systems, In: Mechatronic Systems Techniques and Applications, Gordon and Breach Science Publishers, Amsterdam, 2000, 1–98.

[4] H. B. Pacejka, Modelling complex vehicle systems using bond graphs. Journal of the Franklin Institute, 1985, 319(**1/2**), 67–81.

[5] L. S. Louca, J. L. Stein, D. G. Rideout, Generating Proper Integrated Dynamic Models for Vehicle Mobility Using a Bond Graph Formulation, Proceedings of the 2001 International conference on Bond Graph Modelling (ICBGM'01), Phoenix, AZ, 2001, 33 (**1**), 339–345.

[6] P. J. Gawthrop, Bond graphs: A representation for mechatronic systems, Mechatronics, 1991, 1 (**2**), 127–156.

[7] J. J. Granda, The role of bond graph modelling and simulation in mechatronics systems: An integrated software tool: CAMP-G, MATLAB–SIMULINK, Mechatronics, 2002, 12 (**9–10**), 1271–1295.

[8] P. J Gawthrop, S. A. Neild, A. Gonzalez-Buelga, D. J. Wagg, Causality in real-time dynamic substructure testing. Mechatronics, 2009a, 19 (**7**), 1105–1115.

[9] C. F. Lin, C.Y. Tseng, T. W Tseng, A hardware-in-the-loop dynamics simulator for motorcycle rapid controller prototyping, Control Engineering Practice, 2006, 14 (**12**), 1467–1476.

[10] W. Marquis-favre, S. Scavarda, Bond Graph representation of Multibody Systems with Kinematic Loops, Journal of the Franklin Institute, 1998, 335B (**4**), 643–660.

[11] P. J. Gawthrop, E. Ronco, Estimation and control of mechatronic systems using sensitivity bond graphs, Control Engineering Practice, 2000b, 8

(**11**), 1237–1248.

[12] R. Merzouki, B. Ould-Bouamama, M. A. Djeziri, M. Bouteldja, Modelling and estimation of tire–road longitudinal impact efforts using bond graph approach, Mechatronics, 2007a, 17 (**2–3**), 93–108.

[13] P. J. Gawthrop, R. W. Jones, S. A Mackenzie, Identification of partially-known systems, Automatica, 1992, 28 (**4**), 831–836.

[14] R. Merzouki, K. Medjaher, M. A. Djeziri, B. Ould-Bouamama, Backlash fault detection in mechatronic system, Mechatronics, 2007b, 17 (**6**), 299–310.

[15] B. Ould Bouamama, K. Medjaher, A. K. Samantaray, M. Staroswiecki, Supervision of an industrial steam generator. Part I: Bond graph modelling, Control Engineering Practice, 2006, 14 (**1**), 71–83.

[16] B. Ould Bouamama, K. Medjaher, M. Bayart, A. K. Samantaray, B Conrard, Fault detection and isolation of smart actuators using bond graphs and external models, Control Engineering Practice, 2005, 13 (**2**), 159–175.

[17] E. Suraci, P. Abagnale, D. Amoroso, F. Mariniello, Development and road tests of an ABS control system, International Journal of Vehicle Mechanics and Mobility, 2006, 44, 393–401.

[18] Edgar Sokolovskij, Experimental investigation of the braking process of Automobiles, Transport, 2005, 10(**3**), 91-95.

[19] C.K. Huang, M.C. Shih, Dynamic analysis and Control of an Antilock Brake system for a motorcycle with a camber angle, Department of Mechanical Engineering, National Cheng-Kung University, Tainan, 2009, 49 (**4**), 639-656.

[20] T. K. Bera, K. Bhattacharya, A. K. Samantaray, Evaluation of antilock braking system with an integrated model of full vehicle system dynamics, Simulation Modelling Practice and Theory, 2011, 19(**10**), 2131–2150.

[21] T.K. Bera, K. Bhattacharya, A.K. Samantaray, Bond Graph Model- based Evaluation of a Sliding Mode Controller for a Combined Regenerative and Antilock Braking System, Preceding of the Institute of Mechanical Engineers Part I: Journal of System and Control Engineering, 2011, 225,

918–934.

[22] F. Keinhifer, J. Miller, D. Cebon, Design concept for an Alternative heavy Vehicle ABS system, Vehicle System Dynamics, 2009, 46, 571-583.

[23] C. Lu, M. Shih, Application of the Pacejka Magic Formula on the study of a Hydraulic Antilock Braking System of a Light Motorcycle, Vehicle System Dynamics, 2010, 41 (**6**), 431-448.

[24] D. Capra, E. Galvagno, V. Ondrak, B. Van Leeeuwen, A. Vigliani, An ABS control logic based on wheel force measurement, Vehicle system Dynamics, 2012, 50 (**12**), 1779-1796.

[25] F. Cheli, E. Leo, S. Melzi, E. Sabbioni, Impact OF Smart Tyres on the existing ABS/EBD control systems, Vehicle System Dynamics, 2010, 48, 255-270.

[26] R.S. Sharp, Limit Braking of a high-performance motorcycle, Vehicle System Dynamics, 2009, 47 (**5**), 613-625.

[27] V. Ondrej, J. Svaboda, M. Valasek, P. Steinbour, Influence of deteriorated suspension components on ABS braking, Vehicle System Dynamics, 2008, 46, 969-979.

[28] V. Mills, B. Samuel, J. Wagner, Modelling and analysis of Automotive Antilock Braking System subject to vehicle payload shifting, Vehicle System Dynamics, 2002, 37 (**4**), 283-310.

[29] E. C. Yeh, Y. Chen, Handling Analysis of a Motorcycle with Added Cambering of the Front Frame, International Journal of Vehicle Mechanics and Mobility, 1990, 19, 49–70.

[30] S. M. Cain, N. C. Perkins, Comparison of experimental data to a model for bicycle steady-state turning, International Journal of Vehicle Mechanics and Mobility, 2012, 8, 1341–1364.

[31] X. P. Lu, K. Guo, D. Lu, Y. Wang, Effect of tire camber on vehicle dynamic simulation for extreme cornering, International Journal of Vehicle Mechanics and Mobility, 2006, 44, 39–49.

[32] H. B. Pacejka, Spin: camber and turning, International Journal of Vehicle Mechanics and Mobility, 2005, 43, 3–17.

[33] R. N. Jazar, A. Subic, N. Zhang, Kinematics of a smart variable caster mechanism for a vehicle steerable wheel, International Journal of Vehicle Mechanics and Mobility, 2012, 50(**12**), 1861–1875.

[34] J. Deur, V. Ivanović , M. Troulis, C. Miano, D. Hrovat, J. Asgari, Extensions of the LuGre tyre friction model related to variable slip speed along the contact patch length, International Journal of Vehicle Mechanics and Mobility, 2005, 43, 508–524.

[35] C. Y. Lu, M.C. Shih, An experimental study on the longitudinal and lateral adhesive coefficients between the tyre and the road for a light motorcycle, International Journal of Vehicle Mechanics and Mobility, 2005, 43, 168–178.

[36] S. Fujii, S. Shiozawa, A. Shinagawa, T. Kishi, Steering characteristics of motorcycles, International Journal of Vehicle Mechanics and Mobility, 2012, 50(8), 1277–1295.

[37] G. Trudel, R. L. Kirby, A. C. Bell, Mechanical Effects of Rear-Wheel Camber on Wheelchairs, The Official Journal of RESNA,1995,7,79–86.

[38] A. Dressel, A. Rahman, Measuring sideslip and camber characteristics of bicycle tyres, International Journal of Vehicle Mechanics and Mobility, 2012, 50(8),1365–1378.

[39] R. N. Jazar, A. Subic, N. Zhang, Kinematics of a smart variable caster mechanism for a vehicle steerable wheel, Vehicle System Dynamics, 2012, 50(**12**), 1861–1875.

[40] H. B. Pacejka, Tyre and Vehicle Dynamics, Butterworth-Heinemann, Elsevier, UK, 2006.

[41] R. Rajamani, Vehicle Dynamics and Control, Springer, US, 2006.

[42] R.G. Longoria, A. Al-Sharif, C. B. Patil, Scaled vehicle system dynamics and control: a case study in anti-lock braking, International Journal of Vehicle Autonomous Systems, 2004, 2(**1/2**), 18–39.

[43] M. Oudghiri, M. Chadli, A. E. Hajjaji, Robust fuzzy sliding mode control for antilock braking system, International Journal on Sciences and Techniques of Automatic Control, 2007, 1(**1**), 13–28.

[44] Symbols User's Manual, High Tech Consultants. <http://www.htcinfo.com>.

[45] K. H. Choudhery, Variable camber suspension system, United States Patent, US 6,874,793 B2, 2005.

[46] R. Boston, Vehicle suspension system with a variable camber system, United States Patent, US 7,914,020 B2.

CURRICULUM VITAE

ADITYABIR SINGH

E-Mail: adityabirsingh@gmail.com ~ Mobile +91-9915372154

Professional Profile

Budding Engineering professional pursuing post-graduation in Thermal Engineering from Thapar University, Patiala. Consistent academic record with zeal to learn new concepts quickly and apply innovative ideas for achieving best results. Motivated, self-starter with a passion to succeed and desire to excel in the areas of Engineering and Technology. Strong communication, interpersonal, relationship management and analytical skills.

Academia

- Pursuing Masters in Thermal Engineering from Thapar University, Patiala 2011–13 Batch with CGPA of 9.18 (up to Third Semester).
- Completed Bachelor in Mechanical Engineering from Baba Banda Singh Bahadur Engg. College, Fatehgarh Sahib, PTU in 2011 securing 82.04%.
- Class 12^{th} from Shiwalik Public School, Rupnagar, CBSE in 2007 with 69.4% of marks.
- Class 10^{th} from Shiwalik Public School, Rupnagar, CBSE in 2005 securing 75.6% of marks.

Dissertation

- Bond Graph aided Performance Analysis of Antilock Braking System for a Vehicle with Camber and Fork Angle.

International Conferences

Bera, T. K. and Singh, A. “Bond graph aided performance analysis of antilock braking system for a bicycle vehicle model with camber angle and fork angle”. International Conference on Machines and Mechanisms (iNaCoMM 2013), IIT Roorkee, 2013 (under review).

Internship

- Six weeks Industrial training at DCM Engineering Limited, Asron, Nawanshahr.
- Six months Industrial training at SML ISUZU Limited, Asron, Nawanshahr.

Other skills

- Done certified course in Ultrasonic Testing of engineering components.
- Good command in programming languages like C, C++ and SYMBOLS.

Personal Details

Date of Birth	:	08 November, 1988.
Contact Address	:	#141, Giani Zail Singh Nagar, Rupnagar, Punjab, 140001.
Tel. (Res.)	:	01881-223689.
Languages Known	:	English, Hindi and Punjabi.